FOSSIL ENERGY

186
3/31/80

DR.772

DOE/MC/03260-4

DISPLACEMENT OF OIL BY CARBON DIOXIDE

Annual Report, October 1978—September 1979

Date Published—February 1980

Prepared for the Department of Energy
Under Contract DE-AC21-78MC03260

New Mexico Petroleum Recovery Research Center
Socorro, New Mexico

U. S. DEPARTMENT OF ENERGY

DOE/MC/03260-4
Distribution Category UC-92a

DISPLACEMENT OF OIL BY CARBON DIOXIDE

Annual Report
for the Period
October 1978--September 1979

F. M. Orr, Jr.
J. J. Taber
Principal Investigators
New Mexico Petroleum Recovery Research Center
Socorro, New Mexico

R. J. Watts
Technical Project Officer
Morgantown Energy Technology Center
Morgantown, West Virginia

Date Submitted--December 1979
Date Published--February 1980

Work Performed for the Department of Energy
Under Contract DE-AC21-78MC03260

U.S. DEPARTMENT OF ENERGY

Abstract and Summary

Good progress has been made on all aspects of the carbon dioxide (CO_2) research program at the New Mexico Petroleum Recovery Research Center. Construction of high pressure experimental equipment for measurements of CO_2 displacement efficiency in cores and slim tubes has been completed. A sophisticated apparatus for measurements of phase behavior and fluid properties of mixtures of CO_2 and crude oils has been designed and built. The experimental setup permits a variety of multiple contact phase behavior experiments which explore mixture compositions which realistically model displacement processes at temperatures and pressures of interest. Gas chromatography techniques previously used to characterize crude oils have been extended to allow analyses of mixtures containing CO_2 and hydrocarbons ranging from methane to molecules as heavy as tetracontane (C_{40}). A series of displacements with alcohol-oil-water mixtures, which are analogue systems with useful similarities to CO_2-hydrocarbon systems, have been completed. A one-dimensional CO_2 flooding simulator has been developed which gives excellent agreement between simulated and experimental results for the analogue alcohol-oil-water displacements. Finally, a qualitative analysis is given for the complex phase behavior observed for mixtures of CO_2 and crude oils at temperatures below 50°C and the effects of phase behavior on expected displacement efficiency are calculated. The results indicate that relatively small changes in pressure can be expected to have a strong influence on the efficiency of CO_2 displacements of crude oils.

Contents

List of Tables

Figures

Displacement of Oil by Carbon Dioxide

Introduction

The carbon dioxide flooding research program at the New Mexico Petroleum Recovery Research Center (PRRC) consists of a coordinated set of CO_2-oil displacement experiments, detailed supporting measurements of phase behavior and fluid properties, and, finally, analysis and interpretation of diplacement experiments using computational process models. The effectiveness of a laboratory CO_2 flood depends on a variety of factors: (1) phase behavior of the CO_2 crude oil mixtures, (2) fluid properties (viscosity and density) of the phases which are present during the flood, (3)rock pore structure, (4) dispersion, (5) phase relative permeabilities and (6) viscous fingering. The six factors listed are obviously not unrelated. The local displacement efficiency of a CO_2 flood is generally acknowledged to be strongly dependent on the phase behavior, though there are disagreements as to the details of the dominant effects of component partitioning in CO_2-crude oil systems, particularly at the low temperatures typical of West Texas, New Mexico and West Virginia reservoirs.[1,2,3] There is considerable evidence, however, that mass transfer effects are important,[4,5] that CO_2 efficiently extracts hydrocarbons from crude oils[1,4] and is highly soluble in them,[1,3,6,7] and that the magnitude of component partitioning is strongly influenced by temperature and pressure. Fluid properties also depend on temperature and pressure, but are more strongly influenced, at least in CO_2-crude oil mixtures, by component partitioning.[8] Rock pore structure, phase relative permeabilities and dispersion are all related. Relative permeabilities will depend on phase compositions if low interfacial tensions result. The presence of dead end pores may influence the efficiency with which CO_2 contacts the oil, thus changing the apparent level of dispersion. Phase relative permeabilities and residual saturations must also depend on pore structure. Finally, viscous fingering, the result of unfavorable combinations of fluid properties, may be important even in labotatory core floods,[9] even though the reverse is often assumed.

Because different displacement mechanisms may produce results which are qualitatively similar, core flooding and slim tube displacement results must be carefully interpreted if the details of the displacement mechanism are to be correctly identified. For instance, unfavorable phase behavior, high levels of dispersion and viscous fingering all can act to broaden the transition zone between CO_2 and oil. Because the three effects scale differently, it is important to understand which of the effects is dominating the displacement results.

The approach taken in this project, therefore, is to make independent measurements of phase behavior, fluid properties and properties of the porous medium to be used in displacement experiments, then to use a numerical simulation model to predict the flow behavior observed. It should be noted that this approach avoids the use of adjustable parameters which may or may not have physical significance. Wherever possible, assumptions made in the process model are being tested experimentally. If quantitative agreement between prediction and experiment can be obtained, then the evaluation of the effects of competing mechanisms can proceed with much greater reliability.

The project is organized into four tasks:

(1) Design, build and test high pressure equipment for phase behavior,

fluid property and CO_2 displacement experiments.
(2) Displacement experiments and supporting phase behavior and fluid property measurements.
(3) Mathematical modeling of CO_2 displacement processes.
(4) Application of laboratory results to field problems.

Progress on each task is discussed below.

Task 1. Experimental Equipment

Schematics of the two major pieces of apparatus are shown in Figures 1 and 2. Figure 1 shows the displacement apparatus for the slim tube and core floods, and Figure 2 shows the equipment used to gather supporting phase behavior and fluid property data.

Displacement Equipment

Slim tube displacements and core floods are performed in the same apparatus. Fluid feed pressure measurement and produced fluid sampling systems are shared by the two displacement sections, with obvious savings in equipment costs over two separate pieces of equipment.

Displacing fluid (CO_2) is delivered at a constant rate from a thermostatted supply vessel to either the core holder or to the slim tube. A more detailed sketch of the core holder is given in Figure 3. The core holder is a 4" OD, 2½" ID SAE 4340 steel sleeve 31" in length. The core is prepared for mounting in the core holder by coating it with a thin coat of epoxy resin (Emerson & Cuming Stycast 2762). Stainless steel (316) end plates with a grid for even fluid distribution are held in place initially by the epoxy sealer coat. The core with end plates is then suspended in the holder barrel and the steel end caps threaded onto the barrel. The annulus between the core and the sleeve is then filled with epoxy and cured at a temperature of 250°F for 15 hours. The core holder barrel is very slightly tapered so that the epoxy coated core can be removed and the core and holder reused. Three pressure taps are provided at intermediate locations along the core holder by penetrating the epoxy layer with 1/16" OD stainless steel tubing.

The core holder design was chosen to avoid leakage problems commonly observed when CO_2 is used in rubber sleeve core holders. Rubber sleeve containment is unsatisfactory because CO_2 diffuses easily through the sleeves at high pressure. The pressure taps along the core allow measurement of the differential pressure in the neighborhood of the transition zone, and the progress of the transition zone through the core can be monitored. That data will provide valuable information on total fluid mobility in the transition zone, which in turn provides indirect information about the effect of multiple phase saturations on fluid transport in the transition zone. When coupled with visual observations of the phases flowing through the sight glass at the core exit, the differential pressure data will be used to contstruct, with the aid of the simulator, a picture of the interaction of phase behavior and flow in the transition zone. Finally, the entire core holder is wrapped with heating tape and insulated. Thus, the temperature control system is simpler than a circulating fluid system.

Plumbed in parallel with the core holder is the slim tube, a 40 ft, ¼" ID stainless steel tube packed with 170-200 mesh glass beads (permeability 5800 md).

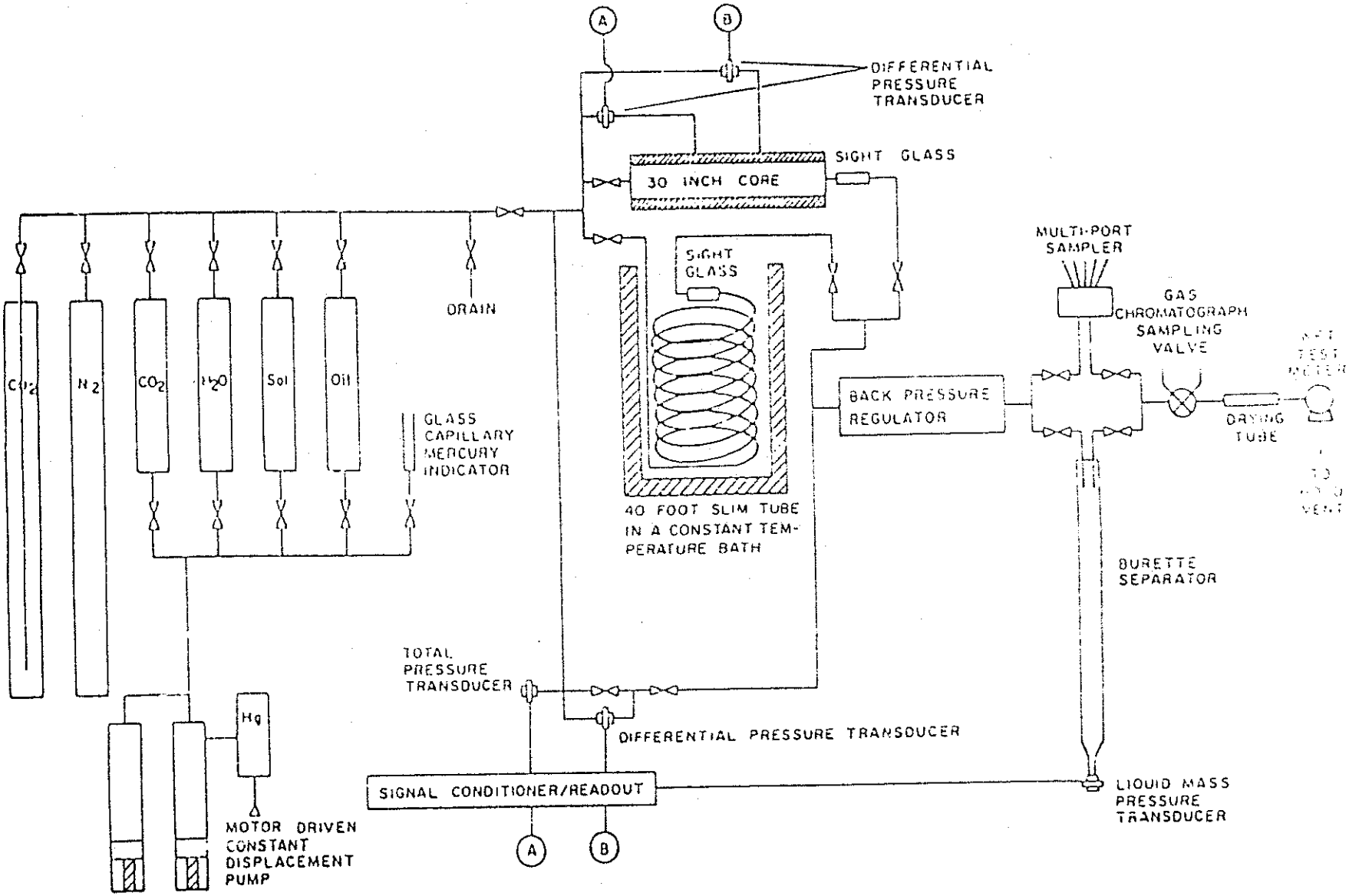

Figure 1 High pressure apparatus for displacement of oil by carbon dioxide in slim tubes and cores.

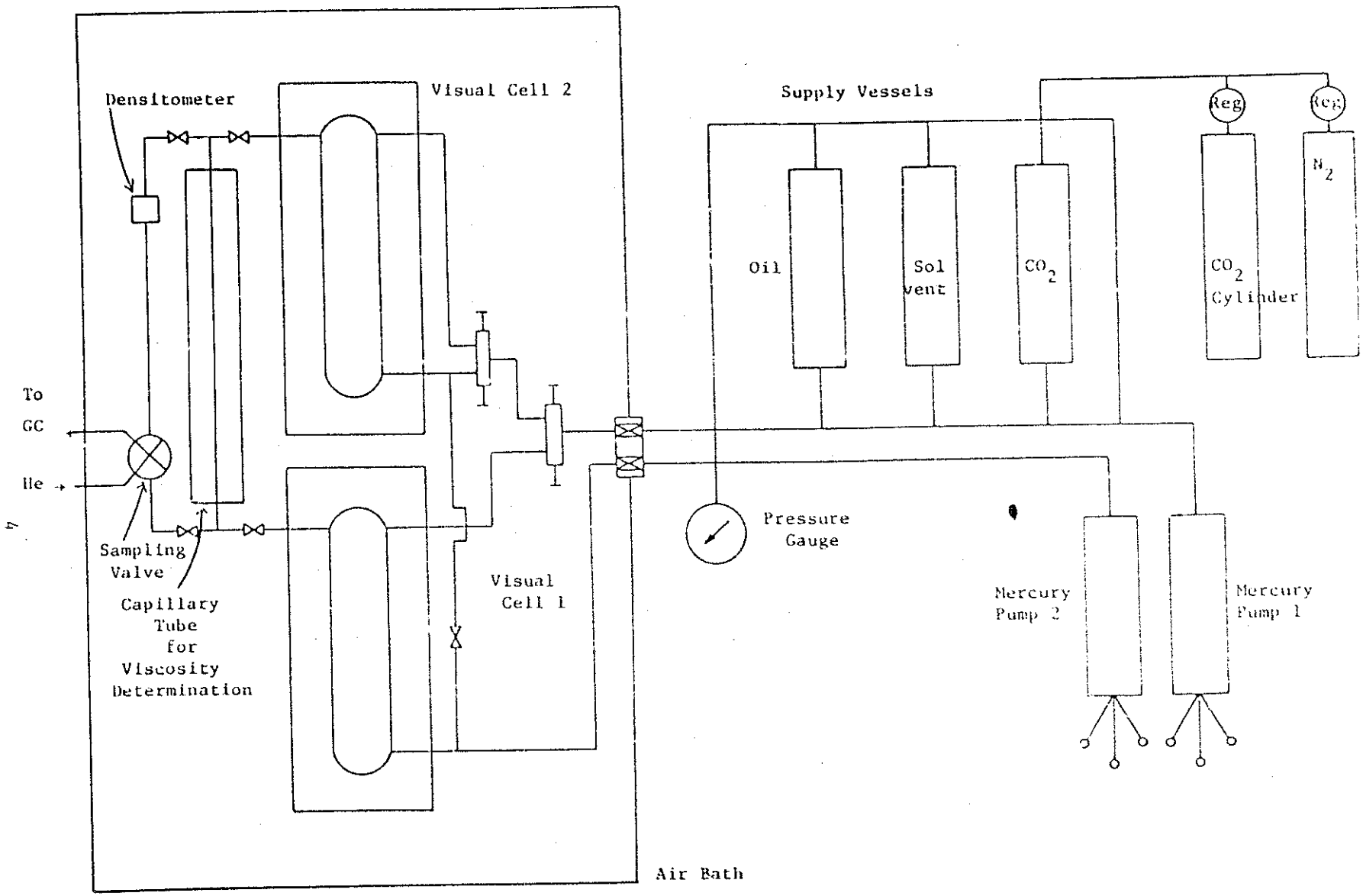

Figure 2 Schematic of equipment for phase behavior and fluid property measurements.

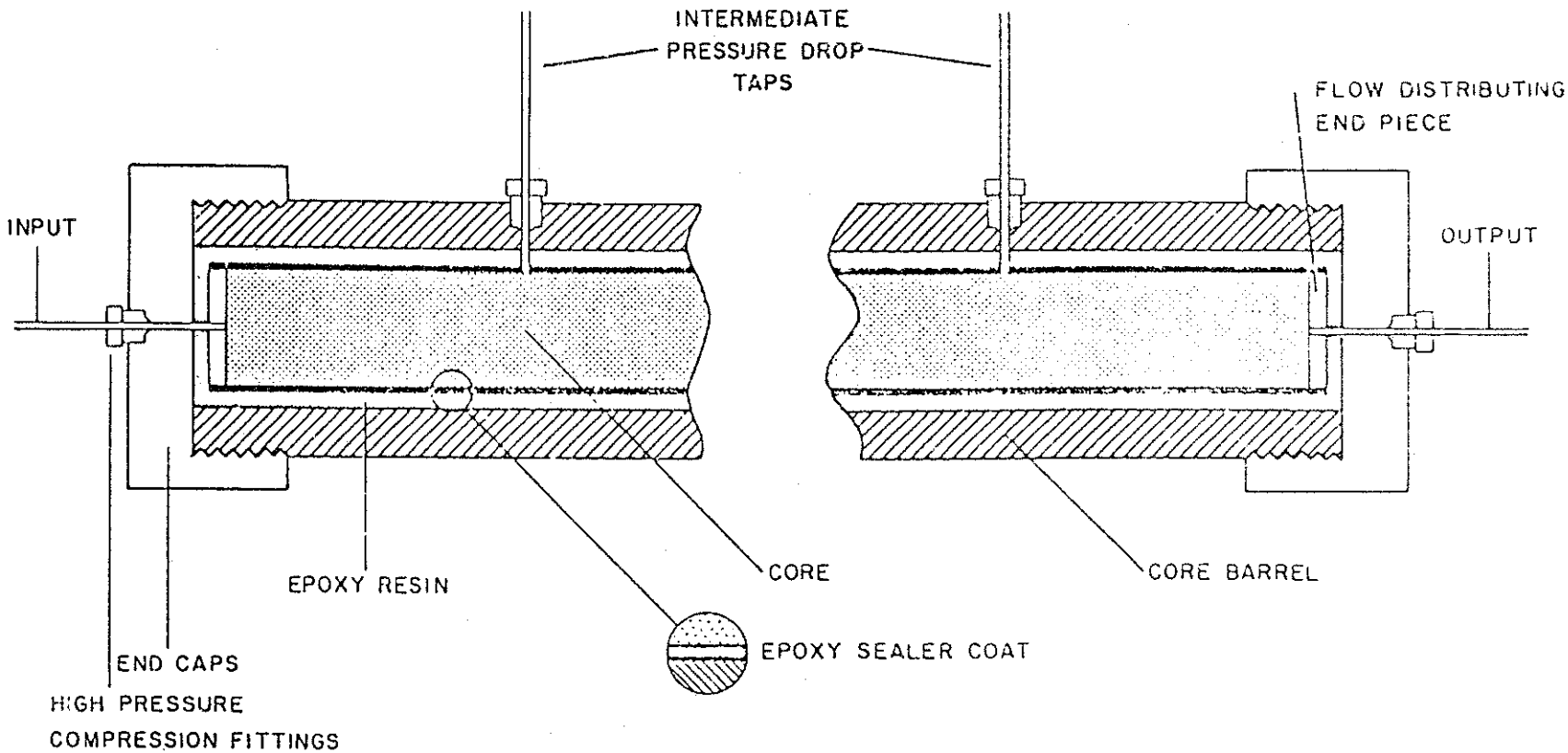

Figure 3 Core holder for high pressure CO_2 displacements.

The 8" coil of tubing is submerged in a water bath, the temperature which can be controlled from ambient to 212°F within ±0.1°F.

Produced fluids are fed to one of two separators. The simpler of the two is a burette which collects produced liquids while the gas is routed to a sampling valve and then to a wet test meter. The mass of liquid produced is recorded automatically using a sensitive pressure transducer to measure the gravity head of the liquid collected in the burette. The second separator uses a multiport switching valve to collect liquid samples for later analysis with produced gas again routed on to the sampling valve and wet test meter.

Produced gas compositions will be measured on-line using the HP 5840 gas chromatograph with an automatic gas sampling valve. Because effluent fluid collection is downstream of the back pressure regulator, the produced gas is at low pressure and will contain CO_2 and hydrocarbon components from methane to pentane with traces of heavier hydrocarbons. Analyses of such mixtures can be completed in a short enough time (10 minutes or less) that adequate resolution of the gas compositions in the transition zone can be obtained. A typical chromatogram is shown in Figure 4 for a gas sample containing air, CO_2, methane, ethane, propane and butane, analyzed on a 1/8" x 4' Porapak Q column. Peak separation is very good so that analysis time could be reduced by increasing the column temperature without reducing the accuracy of the analysis.

Produced liquid samples will be collected for later analysis since an analysis of a liquid sample takes approximately 40 minutes, too long for on-line analysis (a more detailed discussion of the analysis technique for crude oils is given below).

Construction of the displacement apparatus is complete with the exception of the multiport effluent sampler which is being assembled now. Displacements have been conducted in the slim tube and will begin shortly in the Berea cores. Carbonate core displacements will follow later. In a typical displacement experiment, data collected will include cumulative liquid and gas production and differential pressures vs. pore volumes injected. Effluent compositions will be measured for the fluids produced in the transition zone between oil and CO_2, and visual observations will be made of phases leaving the slim tube or core in the capillary sight glass. The compositional data for the produced fluids will be used to make a detailed quantitative test of the accuracy of process model calculations, since the compositions of produced fluids are predicted by the one dimensional flow simulator (see Task 3). It should be noted that the sample collection scheme used here does not allow the determination of the compositions of the phases flowing at high pressure at the exit of the core or slim tube, though overall compositions of the produced fluids are measured. Measurement of the compositions of the phases actually flowing requires sampling at high pressure, an experimental refinement which will be deferred to future projects.

Phase Behavior and Fluid Property Measurements

A schematic of the phase behavior equipment is shown in Figure 2. The standard Ruska air bath has been modified to allow the mounting of two cells, each containing up to two hundred cm^3 of sample. The cells have windows on both sides of the upper half of the cell, and each cell has four sampling ports in the region which can be viewed. Lighting from front and rear will allow examination of the cell contents in both reflected and transmitted light. Both cells are mounted on a single rotating bracket so that the cells can be

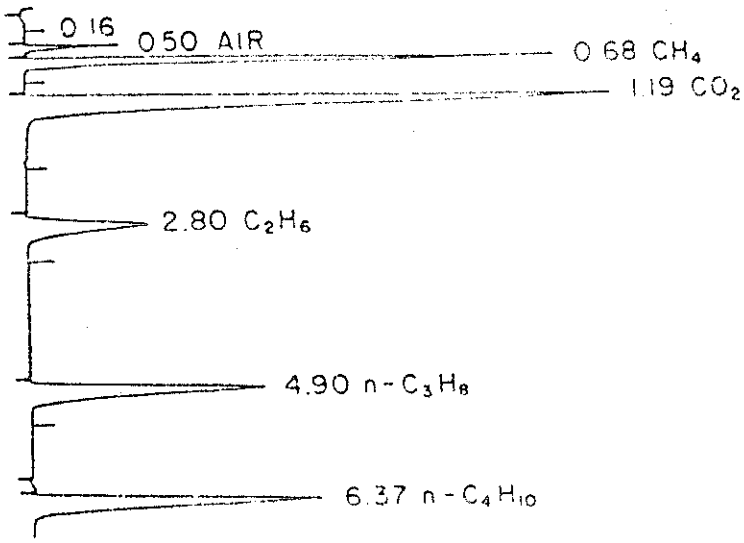

Figure 4 Chromatogram for analysis of mixtures contain CO_2 and light hydrocarbon gases. Analysis was performed on a Hewlett-Packard HP5840 gas chromatograph using a 4 ft. x-1/8" Porapak Q column. Labels given for each peak are retention time (minutes) and component name.

inverted for mixing of the cell contents or viewing or sampling the contents of the lower portion of the cell.

Metered volumes of hydrocarbons or CO_2 can be charged into either of the visual cells. The fluid to be charged is displaced from a supply vessel by mercury from mercury pump 1 while an equal volume of mercury is withdrawn from the visual cell into the barrel of pump 2 (the two mercury pumps are actually a single Ruska pump with two 250 cm^3 barrels). When the CO_2-hydrocarbon mixture has equilibrated, the phase volumes can be measured visually by measuring interface heights. Phase properties are measured by transferring the appropriate phase to visual Cell 2 through a transfer loop which contains capillary tubes for viscosity measurement, a high pressure densitometer (Mettler/Paar DMA 512), and a high pressure sampling valve.

A more detailed sketch of the sampling valve arrangement is shown in Figure 5. Figure 5a shows the valve position for cleaning the high pressure switching valve, V1, a Valco CV-6-UHPA-HC valve capable of withstanding 5000psi at ambient temperatures, and V2, a low pressure, high temperature Valco 4-CV-6-HTA-HC valve rated at 300 psi and 300°C. In this position, solvent can be flushed through the entire sample loop without removing valves from the system. In Figure 4b, the sampling configuration is shown. Valve V1 switches the sample line from the high pressure cells to the sampling valve V2. The phase to be sampled is blown down across a flow restriction into the sample loop (S) in V2. Valve V2 is then switched to the position shown in Figure 4c to flush the sample on column. Valve V2 is maintained at 300°C to vaporize all but the heaviest components of the mixture.

The sampling arrangement shown in Figure 5 is dictated by the fact that sampling values are not available which can withstand both high pressure, required because the samples are at high pressure, and high temperature, required to flush the heaviest hydrocarbon components present in the sample into the gas chromatograph. Performance testing of the sampling system will be underway shortly.

The double cell arrangement described here offers important advantages for the type of experiments being planned:

- Measurements of density and viscosity can be made without removing large samples. This means that the density and viscosity experiments will not alter the overall composition in the system. Thus, numerous measurements can be made without cleaning and reloading the cell.
- Sampling for measurement of phase compositions will take only microliter size samples so that overall compositions are altered negligibly. Displacement of the phase to be sampled through the sampling valve should provide more representative samples than drawing samples into an evacuated container. However, the accuracy of the sampling system remains to be tested.
- A variety of multiple contact phase behavior experiments, similar to those described by Gardner, Orr and Patel[1], can be performed in this apparatus. For instance, a two-phase CO_2-hydrocarbon mixture can be made in Cell 1 and the upper phase transferred to Cell 2 and mixed with fresh oil. Repeated contacts of the CO_2 rich upper phases with fresh oil will simulate the multiple contact process which occurs at the leading edge of a CO_2 flood. Phase behavior near the trailing edge of the transition

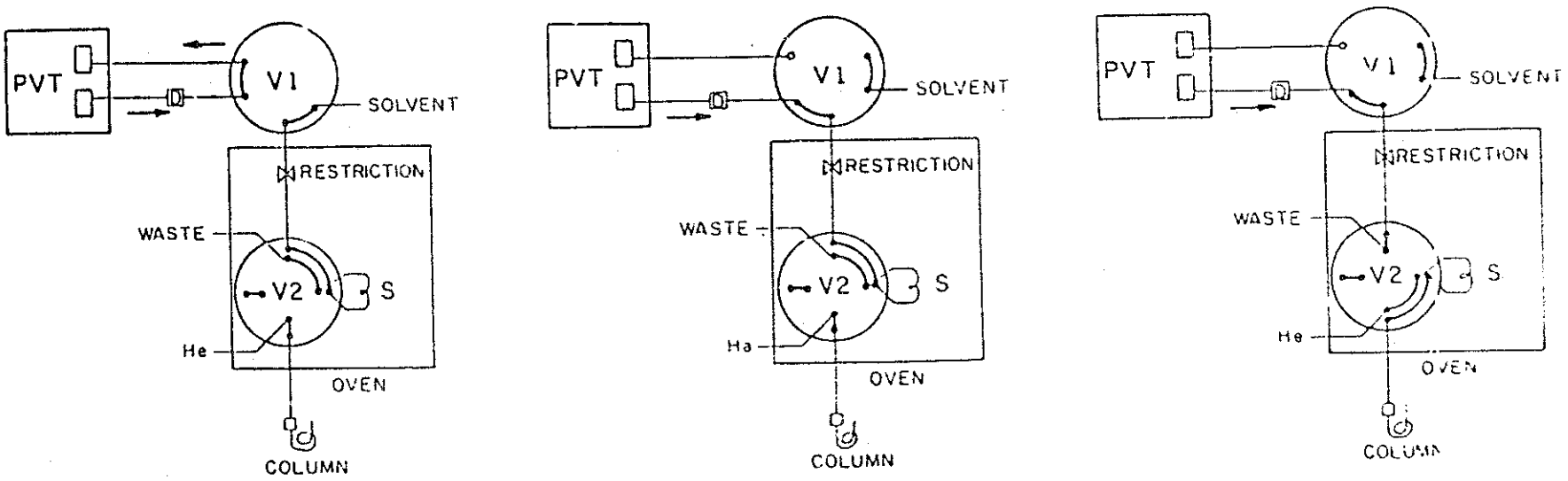

a. Clean

b. Load Sample

c. Inject Sample

Figure 5 Valve positions for high pressure sampling and sample injection into the gas chromatograph.

zone can be examined by contacting the oil rich lower phase, which remains after removal of the CO_2 rich upper phase, with fresh CO_2. Multiple contacts of the remaining oil phase will study the extraction of hydrocarbons by CO_2. Both types of experiments will provide new information about the phase behavior and fluid properties of mixtures which are likely to develop during field displacements. The data to be collected should approximate much more closely the composition paths of actual displacements than have the binary mixture phase behavior experiments most often performed in past CO_2 flooding research.

Chemical Analysis of CO_2-Crude Oil Mixtures

Most phase compositions reported for CO_2-crude oil mixtures do not resolve amounts present of components heavier than heptanes (C_7), probably because standard low temperature fractional distillation techniques analyze only out to "heptanes-plus" (C_{7+}) with extensions to "undecanes-plus" (C_{11+}) possible without too much difficulty. Nevertheless, where more detailed analyses have been reported,[1,4,6] experimental results clearly indicate that, under appropriate conditions of temperature, pressure and composition, CO_2 can extract hydrocarbons as at least as heavy as eicosane (C_{20}). Thus, it appears that the traditional definition of intermediates, which play a key role in development of miscibility, as C_2-C_6 hydrocarbons is not sufficiently broad. More detailed analysis of CO_2-crude oil mixtures would help to improve understanding of the role of component partitioning in the generation of miscibility, would aid in the choice of pseudo-components for process simulation, and may be necessary for adequate representation of phase behavior with an equation of state.[11]

Gas chromatography offers a convenient method for more detailed analyses if several uncertainties can be resolved. First, the analysis technique must be able to adequately separate mixtures containing CO_2 and hydrocarbons of widely different molecular weights, in some cases from methane to the heaviest components eluted. Second, some estimate of amounts not eluted must be made. Finally, and perhaps most difficult, representative samples of the mixture to be analyzed must be obtained from the high pressure cell and transported to the chromatograph. Techniques being tested to resolve these uncertainties are described below.

Chromatography offers several clear advantages over distillation methods. The analysis time is about forty minutes instead of hours, and the repeatability and precision are much better. Chromatography requires a sample size of only a few microliters vs. milliliters for distillation. A disadvantage to chromatography is that cuts are not available for further characterization (molecular weight, specific gravity, refractive index).

The proposed ASTM method for gas chromatographic analysis of crude oils[12] provides the basis for the analysis of CO_2-crude oil mixtures. Extensions of the proposed method are required to handle CO_2 and the light ends, methane through butane so that one analysis can be used to characterize mixtures containing CO_2 and hydrocarbons ranging all the way from methane to C_{40}. Some separation of the methane and CO_2 peaks can be obtained using a 1/4 in. x 24 in. column packed with UCW 982 silicone rubber on chromosorb PAW, as shown in Figure 6a by starting the analysis at -65° C and increasing the column temperature 10°C/min. The separation between the CO_2 peak and the small ethane peak is much less satisfactory

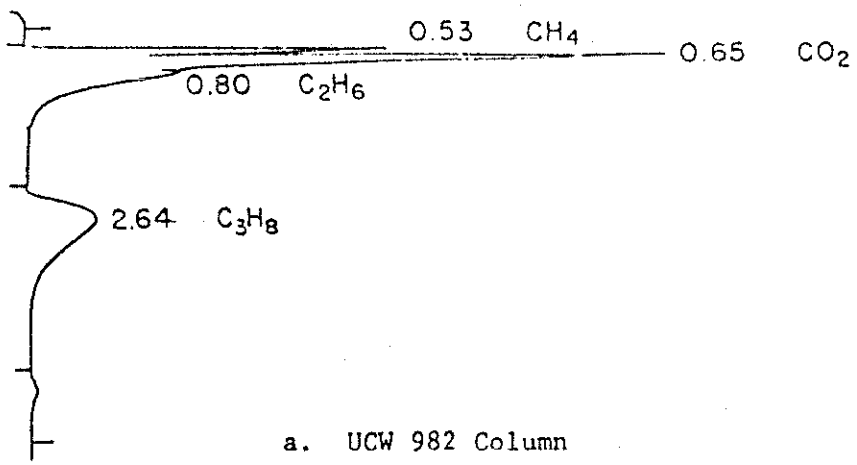

a. UCW 982 Column

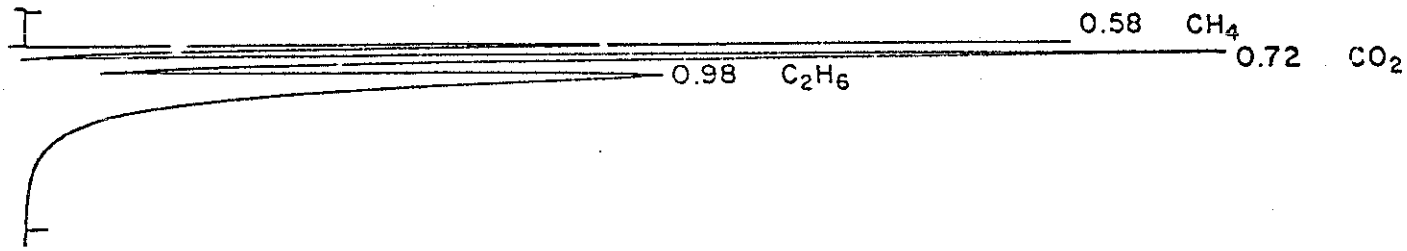

b. OV-101 Column

Figure 6 Comparison of separations of CO_2 and light hydrocarbons using UCW 982 and OV 101 columns.

however. A much better separation is obtained using 1/8" x 6' OV 101 column as shown in Figure 6b. This analysis was begun at -65°C with the temperature held constant. A combination of temperature programming and a slightly higher starting temperature (say 55°C) will reduce tailing of the ethane peak. The OV 101 column offers an additional advantage in that it shows much lower column bleed at the 370°C, the end point temperature for the simulated distillation. It appears, therefore, that an analysis sequence is now available which can report a boiling point of distribution (and hence an approximate carbon number distribution) for CO_2 hydrocarbon mixtures of very wide molecular weight ranges and which can be obtained without using column switching or backflushing.

Estimation of the amount of heavy hydrocarbons not eluted requires a second run in which a measured amount of internal standard (a mixture of normal paraffins C_{14}, C_{15}, C_{16} and C_{17}) has been added.[12] Identical sample amounts are injected in the two runs. The differences in integrated areas and the areas of the standard peaks can be used to construct an estimate of the amount of material not eluted. An example of the resulting carbon number distribution for Maljamar crude oil (supplied by Continental Oil Company) is shown in Figure 7. This technique can not be used for samples obtained from the high pressure liquid sampling valve, but can be used to characterize the original crude oil and any samples for which sufficient quantities are withdrawn that a mixture of the sample and standard can be prepared.

Task 2. Displacement Experiments

High pressure core flood and slim tube displacement experiments are just getting underway with the completion of equipment construction. Floods will be conducted using both crude oils and mixtures of well-characterized hydrocarbons. Crude oil displacements offer the final test of understanding of the displacement and of the accuracy of process model calculations. Displacements in well-characterized systems offer several experimental and theoretical advantages. The complexity of compositional analyses is reduced, and the phase behavior can be accurately represented by an equation of state,[13] so that the phase compositions and saturations existing during the flood can be reconstructed with greater accuracy than is currently possible for crude oil systems. Detailed data for such a system which behaves qualitatively like CO_2-crude oil systems would be of great value for testing simulators currently being written to model CO_2 flooding processes.[14,15,16] Only one such test has been attempted,[17] but the well-characterized hydrocarbon mixture[2] was so light (molecular weight 108) that the phase behavior observed was quite different from that observed for CO_2-crude oil systems. Investigations are underway to build a test oil composed of a small number of well-characterized hydrocarbons which produces phase behavior like that observed for CO_2-crude oil systems.

During construction of the displacement apparatus, a series of low pressure analogue displacements were run in a very simple glass bead pack apparatus shown schematically in Figure 8. The bead pack is saturated with the mixture to be displaced, and the displacing phase is injected at a constant rate by a syringe pump. Produced fluids are collected in vials for later analysis by gas chromatograph.

The displacement experiments were designed to provide a quantitative test of the accuracy of the one dimensional process simulator being developed concurrently for the simplest of flow systems in which phase behavior is important. Displacement tests have been performed for two alcohol-hydrocarbon-water systems, phase diagrams for which are shown in Figures 9 and 10. Phase compositions shown in Figures 9 and 10 were determined by gas chromatography. Figure 9 shows the two-phase region and tie lines for mixtures of iso-octane (IC_8), iso-propanol (IPA)

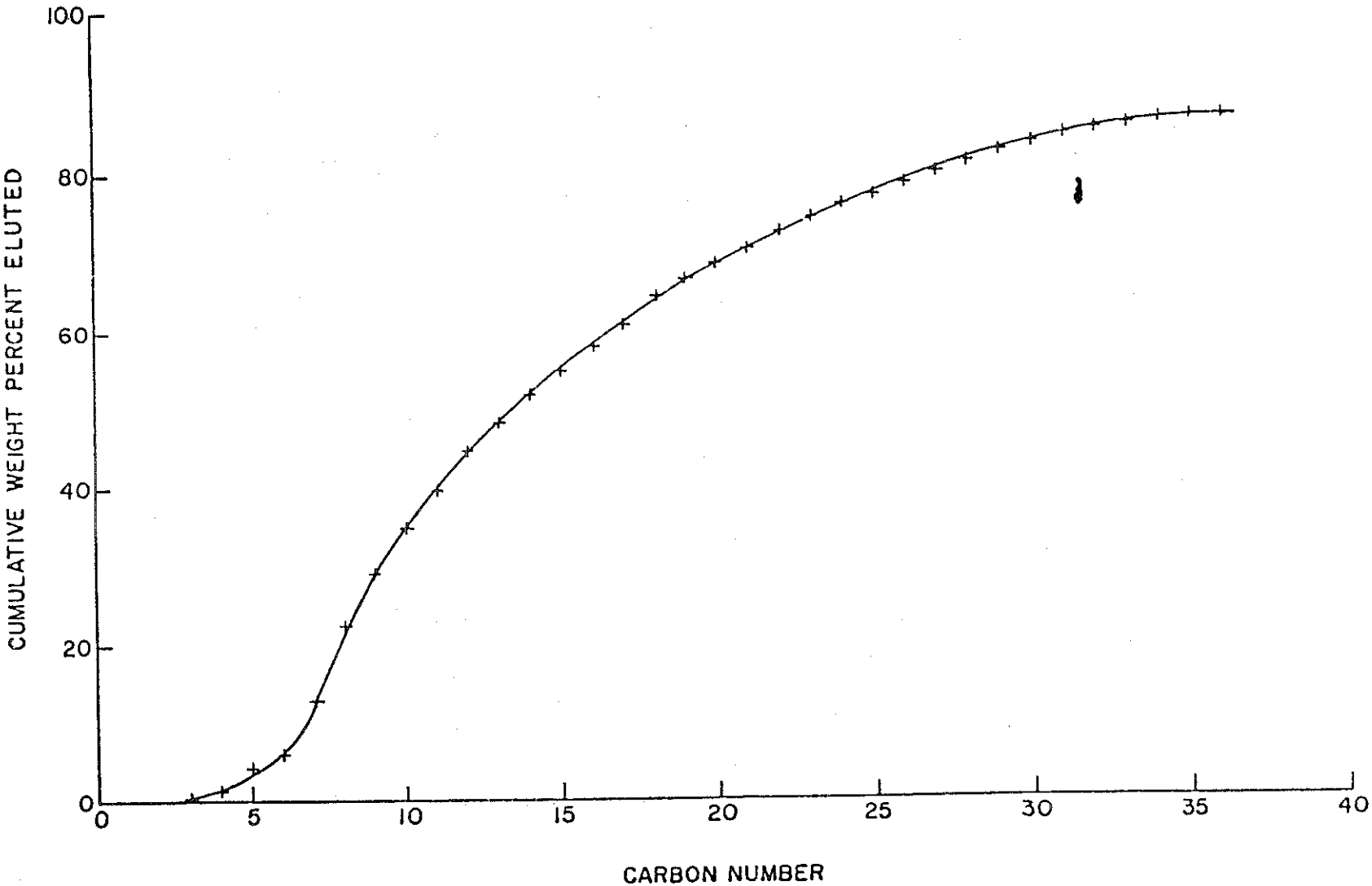

Figure 7 Results of a simulated distillation run for separator liquid from the Maljamar field, Eddy and Lea Counties, New Mexico.

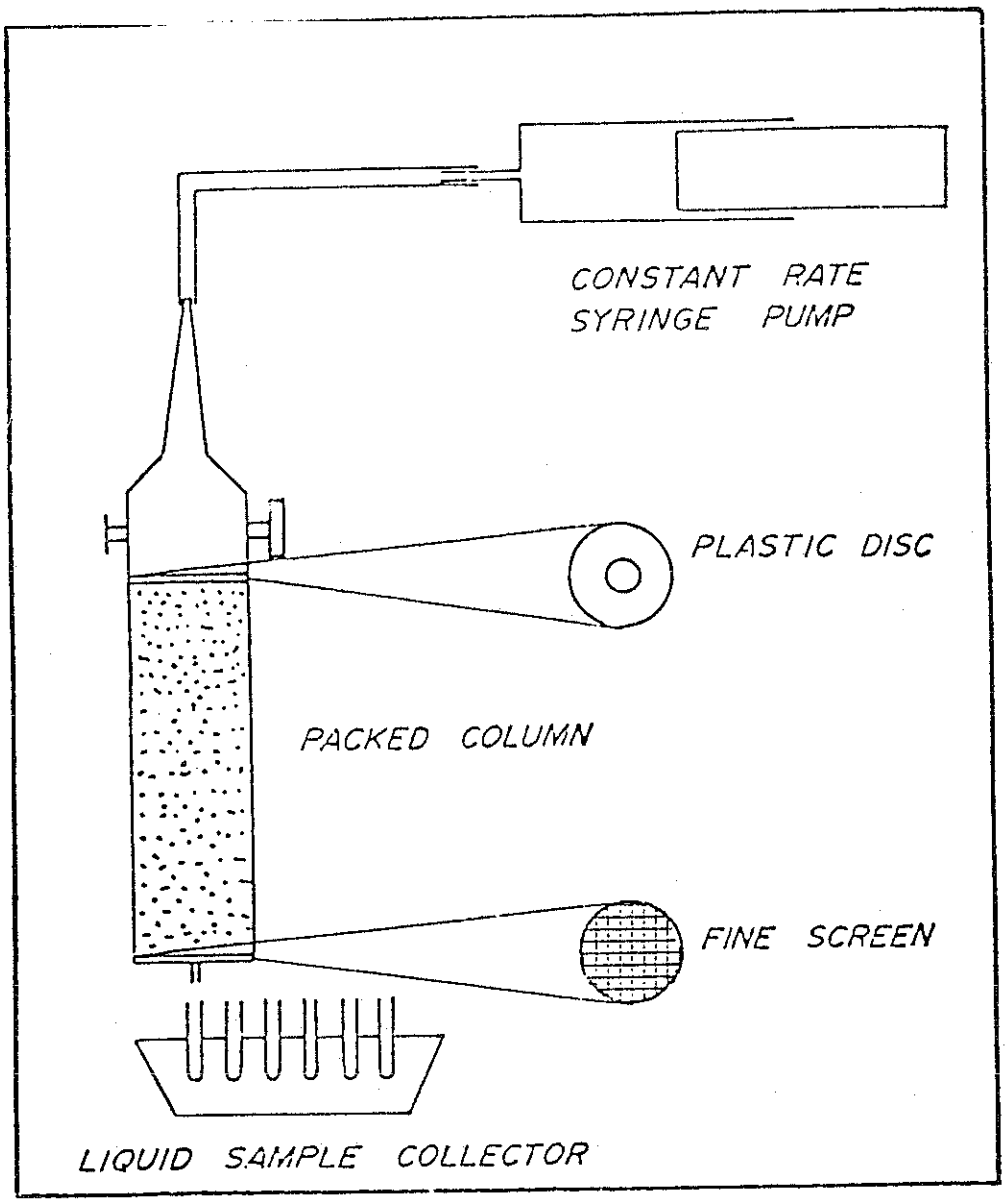

Figure 8 Schematic of the bead pack displacement apparatus used for analogue displacements of water-oil-alcohol systems. The bead pack is 30 cm in length.

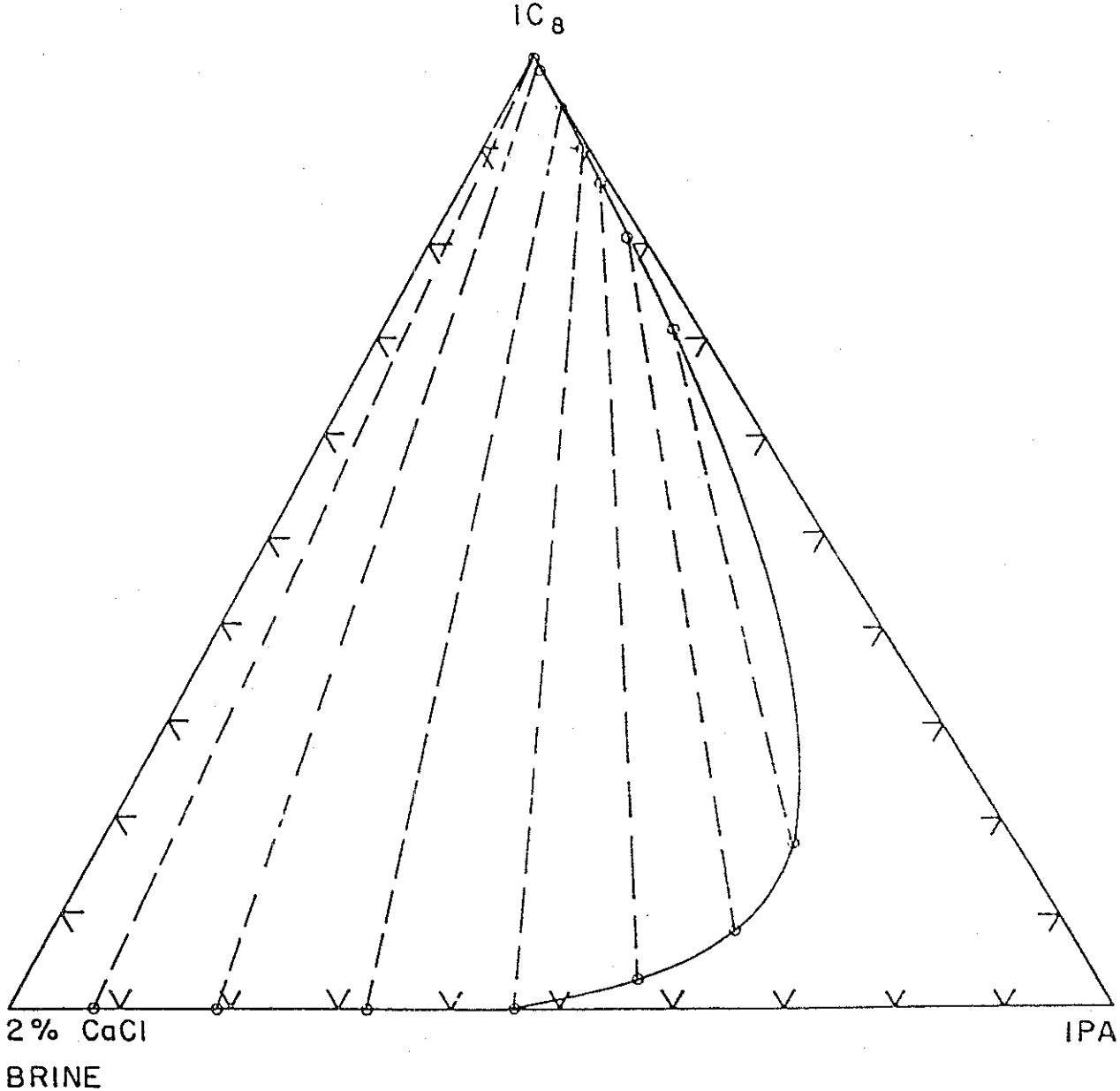

Figure 9 Place behavior of iso-octane-iso-propanol-brine (2 wt.% $CaCl_2$ mixtures. Compositions are in volume fractions. Dashed lines are equilibrium tie lines determined by gas chromatography.

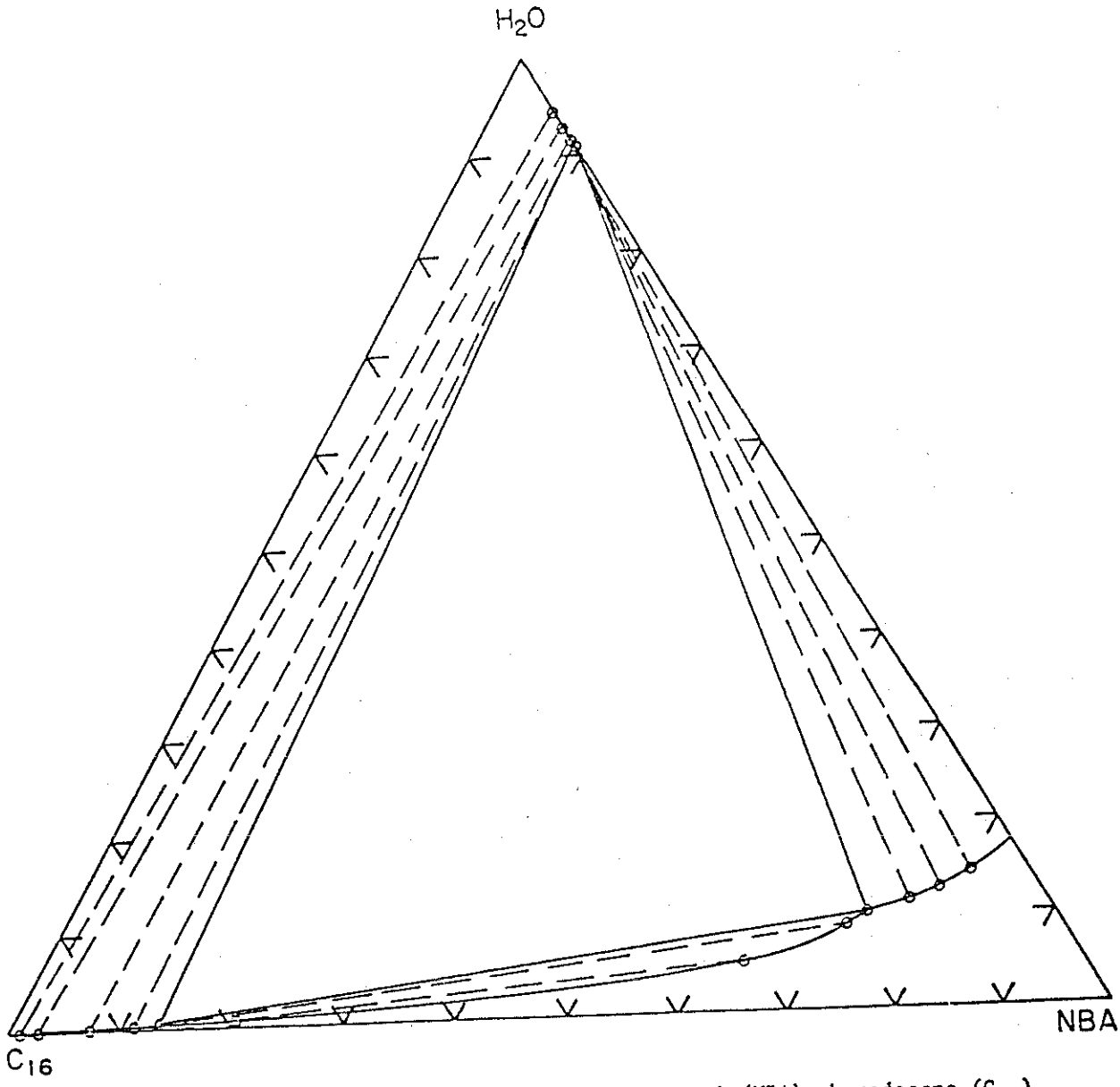

Figure 10 Phase behavior of water (H_2O), n-butanol (NBA), hexadecane (C_{16}) mixtures. Compositions are in volume fractions. Dashed lines are equilibrium tie lines determined by gas chromatography. Any mixture with an overall composition lying within the large triangle in the center of the diagram forms three phases with compositions of the vertices of the three phase triangle.

and brine (2 wt. % $CaCl_2$). Figure 10 shows similar data for mixtures of water (H_2O), n-butanol (NBA) and n-hexadecane (C_{16}). This true ternary system exhibits three phases, as do low temperature CO_2-crude oil mixtures,[1,2,10] and thus offers an opportunity to test the accuracy of simulation of the interaction of more complex phase behavior with flow in a simple porous medium. Density and viscosity data for both systems are shown in Table 1. Compositions of displaced and displacing phases for floods conducted so far are given in Table 2, along with breakthrough and ultimate recovery results. Recovery curves and composition paths for the two phase displacements (brine-IPA-IC_8) are compared with computed recovery curves in the discussion of simulation results under Task 3.

The displacements described in Table 2 cover phase behavior ranging from completely immiscible to first contact miscible and include floods in which miscibility is generated by vaporization (extraction). Thus, they provide a stringent test of the capability of the simulator to handle the interaction of phase behavior with multiphase flow. Run 1, displacement of brine by IC_8 was a completely immiscible displacement. Runs 2 and 3 included effects of phase behavior but did not develop miscibility. They illustrate that phase behavior can increase recovery even when development of miscibility is not complete. Run 4 generated a miscible displacement via a vaporization (extraction) mechanism as did run 6 and run 5 as first contact miscible. Run 7 was used to measure the dispersion coefficient for the bead pack and was first contact miscible. Run 8 was a three phase displacement which proved remarkably efficient.

Sample results from run 8 are shown in Figures 11 and 12. Figure 11 plots recovery of NBA and C_{16}, the components of the analogue oil, as a fraction of the amount in place at the start of the displacement. Also plotted is the amount of water produced (in pore volumes). Figure 12 plots the overall compositions of collected samples of the produced fluids. Compositions were determined by gas chromatography. In this run, three phases were observed in the produced fluids after breakthrough as indicated by the fact that the overall compositions of the produced fluids lie within the three phase triangle. Details of runs 1-5 are reported under task 3 where they are compared with simulation runs.

Task 3. Mathematical Modeling of CO_2 Displacement Processes.

One Dimensional Simulator

A one-dimensional process simulator has been written which models multiphase flow with component transfer between phases. The simulator is based on the following assumptions:

1. Local chemical equilibrium exists between phases.
2. There is no volume change on mixing.
3. Capillary pressure effects are negligible.
4. Darcy's law governs flow in the one dimensional flow system of uniform properties.
5. Changes in pressure over the length of the displacement have negligible effect on the phase behavior of the hydrocarbons and CO_2.

Table 1. Fluid Properties of Alcohol-Oil-Water Systems at 25°C

Mixture Composition (Vol. %)			Density	Viscosity
IC_8	IPA	Brine	g/cm³	cp
100.00	—	—	0.688	0.479
—	100.00	—	0.7812	2.08
—	—	100.00	1.0142	0.949
—	21.11	78.89	0.991	1 956
—	35.06	64.94	0.967	2.707
0.65	46.48	52.87	0.941	3.095
2.80	55.55	41.65	0.905	3.337
7.82	61.87	30.31	0.868	3.159
16.68	62.90	20.42	0.830	2.548
98.77	1.14	0.09	0.69	0.4[illegible]3
93.82	5.37	0.81	0.694	0.486
89.35	9.58	1.07	0.697	0.505
84.89	13.51	1.60	0.701	0.533
79.04	18.73	2.23	0.707	0.581
70.14	26.92	2.94	0.719	0.692
—	10.00	90.00	1.002	1.346
—	20.00	80.00	0.9884	1.873
—	30.00	70.00	0.9724	2.508
—	40.00	60.00	0.9514	2.858
—	50.00	50.00	0.9275	3.114
—	60.00	40.00	0.9019	3.158
—	70.00	30.00	0.8755	3.058
—	80.00	20.00	0.8472	2.769
—	90.00	10.00	0.8170	2.370
H_2O	NBA	C_{16}		
100.00	—	—	0.9971	0.8937
—	100.00	—	0.8061	2.56
—	—	100.00	0.7701	3.05
0.66	13.30	86.04	0.7746	2.79
10.60	72.24	17.16	0.8221	2.82
91.27	8.73	—	0.9864	1.18
17.51	82.49	—	0.8440	2.85
12.76	77.99	9.25	0.8304	2.80
—	75.00	25.00	0.7956	2.58
—	50.00	50.00	0.7859	2.55
—	25.00	75.00	0.7770	2.62

Table 2. Summary of Displacement Tests

Run	Displacing Phase Composition (Vol.%)			Displaced Phase Composition (Vol.%)			Breakthrough Recovery (%PV)	Recovery at 1.7 Pore Volume Injected (%)			
	IC_8	IPA	Brine	IC_8	IPA	Brine		IC_8	IPA	Brine	
1	100	-	-	-		100	64.15	-	-	71.00	Immiscible
2	100	-	-	-	50	50	55.00	-	88.00	68.00	immiscible
3	100	-	-	-	75	25	68.00	-	93.00	78.00	immiscible
4	100	-	-	-	85	15	70.00	-	99.30	91.20	developed miscibility
5	100	-	-	-	90	10	72.00	-	99.80	97.50	developed miscibility
6	-	-	100	70	30	-	63.83	85.90	91.00	-	developed miscibility
		C_8H_{10}*		IC_8	C_8H_{10}*			IC_8	C_8H_{10}		
7		100		5	95		98.00	100	100		first contact miscible
	H_2O	NBA	C_{16}	H_2O	NBA	C_{16}		H_2O	NBA	C_{16}	
8	100	-	-	-	50	50	72.76	-	96.40	87.17	immiscible

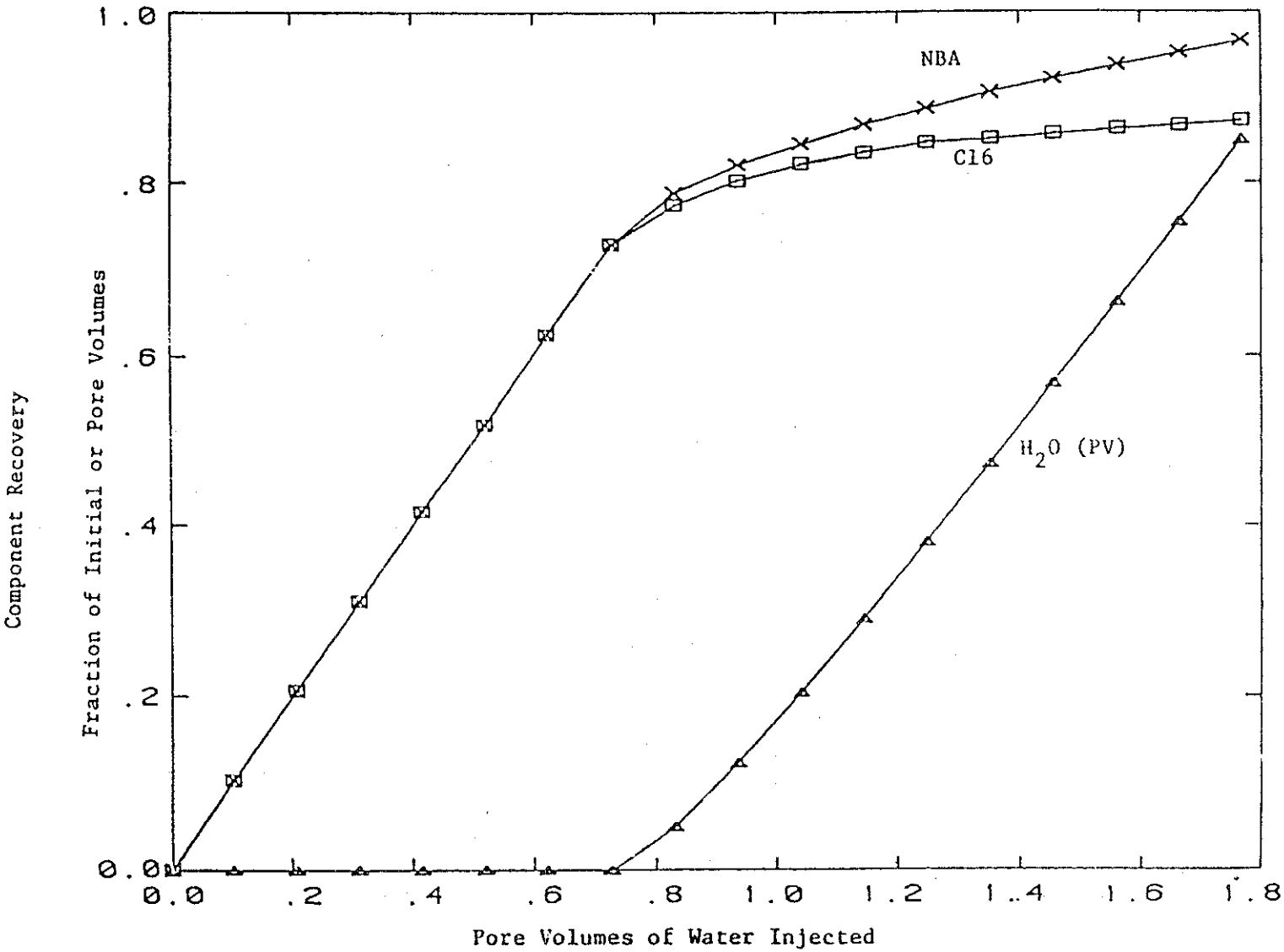

Figure 11 Run 8 : Experimental component recovery for displacement of 50 vol. % hexadecane (C_{16}) - 50 vol. % n-butanol(NBA) by water(H_2O). Recovery of NBA and C_{16} are plotted as fractions of the amount originally in place in the bead pack. H_2O production is in pore volumes (PV).

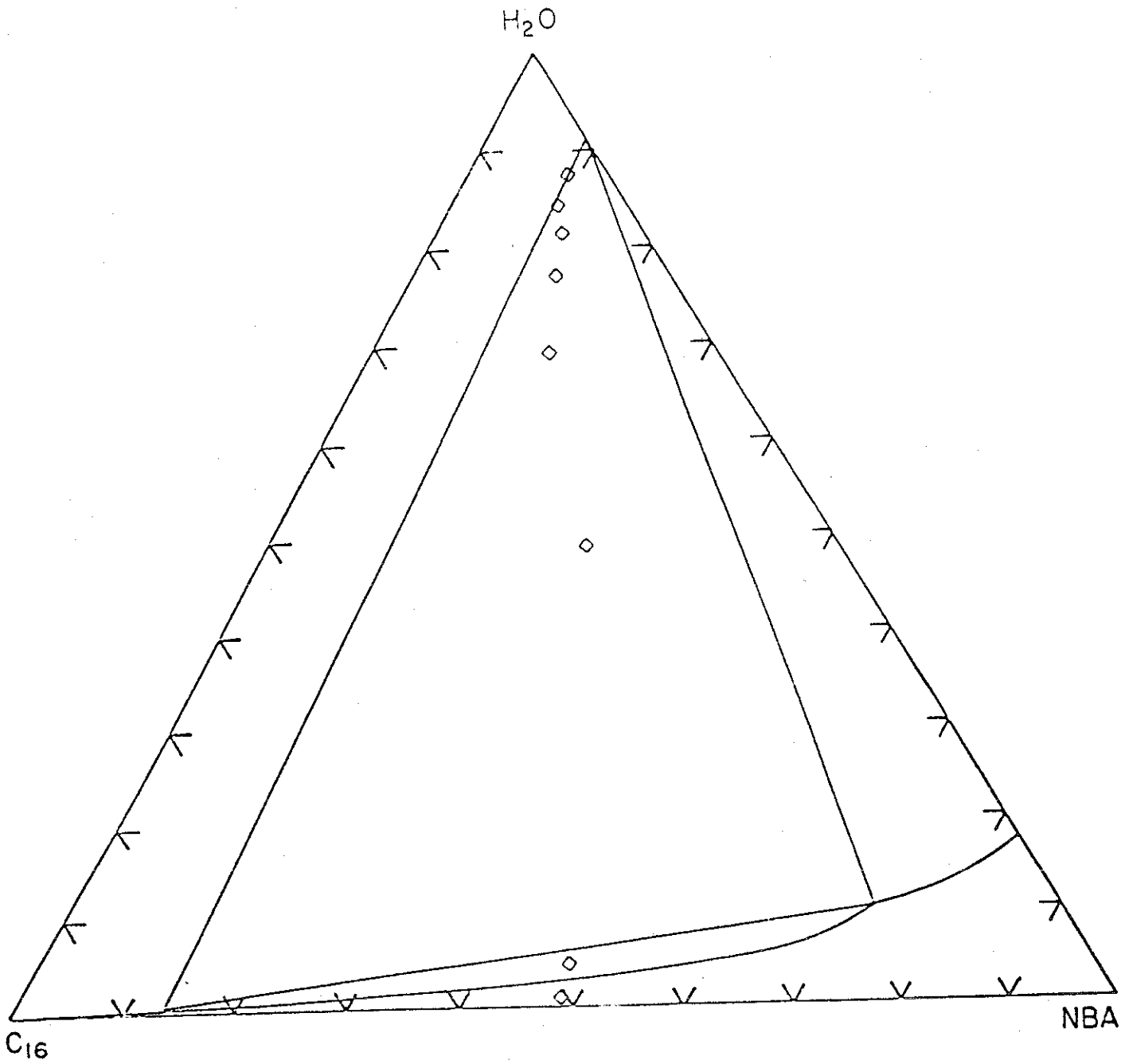

Figure 12 Run 8: Overall compositions of produced fluids. Overall compositions are calculated from measurements of produced phase volumes and compositions. Production of three phases occurred during much of this run.

6. Physical dispersion can be modeled by numerical dispersion. These assumptions are similar to those used by Pope and Nelson in the development of a compositional simulator for chemical flooding,[18] and the approach to the representation of the phase behavior in terms of pseudo-components is similar to that described by Gardner, Orr and Patel.[1]

There is little direct evidence to support assumption 1, though estimates of diffusion times on a pore scale suggest that the assumption is reasonable. Nelson and Pope[19] and Nelson[20] concluded that the local equilibrium assumption is justified for chemical flooding applications. Assumption 2 is perhaps the most questionable. It is clearly violated when the CO_2 density is gas like, but when the CO_2 density is near that of the oil, the assumption appears reasonable, at least when the methane concentration is low.[1] A revised version of the simulator which relaxes that assumption is being written. Assumption 3 is untested; no data are available to assess the magnitude of capillary pressures for the phases present in a CO_2 flood. Hence, it is reasonable to neglect capillary pressure effects as a first step. Darcy's law is not in question (assumption 4), but the generalization of Darcy's law to four phase flow (water plus three phases containing hydrocarbon plus CO_2) is not obvious. Calculation of three phase relative permeabilities is open to question[21] and the extension to four phases requires testing. Assumption 5 can be satisfied by choosing experimental displacement velocities close to field values. Assumption 6 must also be tested (see below).

Pure convection of multiple phases in a one-dimensional porous medium is described by [18]

$$\frac{\partial}{\partial \tau} \sum_{j=1}^{n_p} C_{ij} S_j + \frac{\partial}{\partial \xi} \sum_{j=1}^{n_p} C_{ij} f_j = 0 \qquad (1)$$

where C_{ij} = volume fraction of component i in phase j,

S_j = saturation of phase j,

f_j = fractional flow of phase j,

ξ = dimensionless distance, $\frac{X}{L}$, $0 \leq \xi \leq 1$,

n_p = number of phases, $1 \leq n_p \leq 4$

and τ = dimensionless time (pore volume)

$$= \int_0^t \frac{q}{LA\phi}\, dt$$

where q = flow rate

L = length

A = core face area

ϕ = porosity

Equation (1) is solved by a fully explicit finite difference method.[18]

As written, the simulator follows four components: CO_2, a light hydrocarbon component, a heavy hydrocarbon component and water. Water is assumed to exist in the separate phase which contains none of the other components. The remaining three components may partition between two additional phases.

The assumption of local chemical equilibrium is implemented by representing the binodal curve on a ternary diagram in terms of piecewise continuous polynomials (see Figure 13). Six pieces of quadratic in component 1 are fitted through points 1,2,and 3, points 3,4,and 5, points 6, 7,and 8, and points 8, 9,and 10, points 11, 12, and 13 and points 13,14, and 15. Tie lines are represented by dividing the phase diagrams into three regions (I, II and III on Figure 13) within each of which all tie lines are assumed to pass through a single point when extended.[22] The three phase region is the triangle labeled region IV. Regions II and III may extend all the way to the edge of the diagram, as does region I. If so, points 5 and 6 and points 10 and 11 are not identical. If those pairs of points are identical, they are taken as the plait point compositions for the respective regions. Thus, all phase behavior for a system can be entered into the simulator by specifying fifteen points on the binodal curve.

Phase fractional flows are given by

$$f_j = \frac{k_{rj}/\mu_j}{\sum_{l=1}^{n_p} k_{rl}/\mu_l} \left(1 - \frac{kAg\sin\alpha}{q} \sum_{i=1}^{n_p} \frac{k_{ri}}{\mu_i} (\rho_i - \rho_j) \right) \qquad (2)$$

where k_{rj} = relative permeability to phase j

μ_j = viscosity of phase j

k = permeability

A = core cross-sectional area

α = dip angle

and g = gravitational acceleration

Three phase relative permeabilities are computed using Stone's second model[22] with modifications suggested by Dietrich and Bondor.[21] When four phase relative permeabilities are required, as may be the case when CO_2-crude oil mixtures are flowing in the presence of water, oil and gas relative permeabilities are computed using Stone's model with the assumption that the two hydrocarbon bearing phases which differ least in composition share the relative permeability of either the oil or gas, whichever is appropriate, in proportion to their saturations. This assumption is not particularly satisfying, and other approaches are being explored.

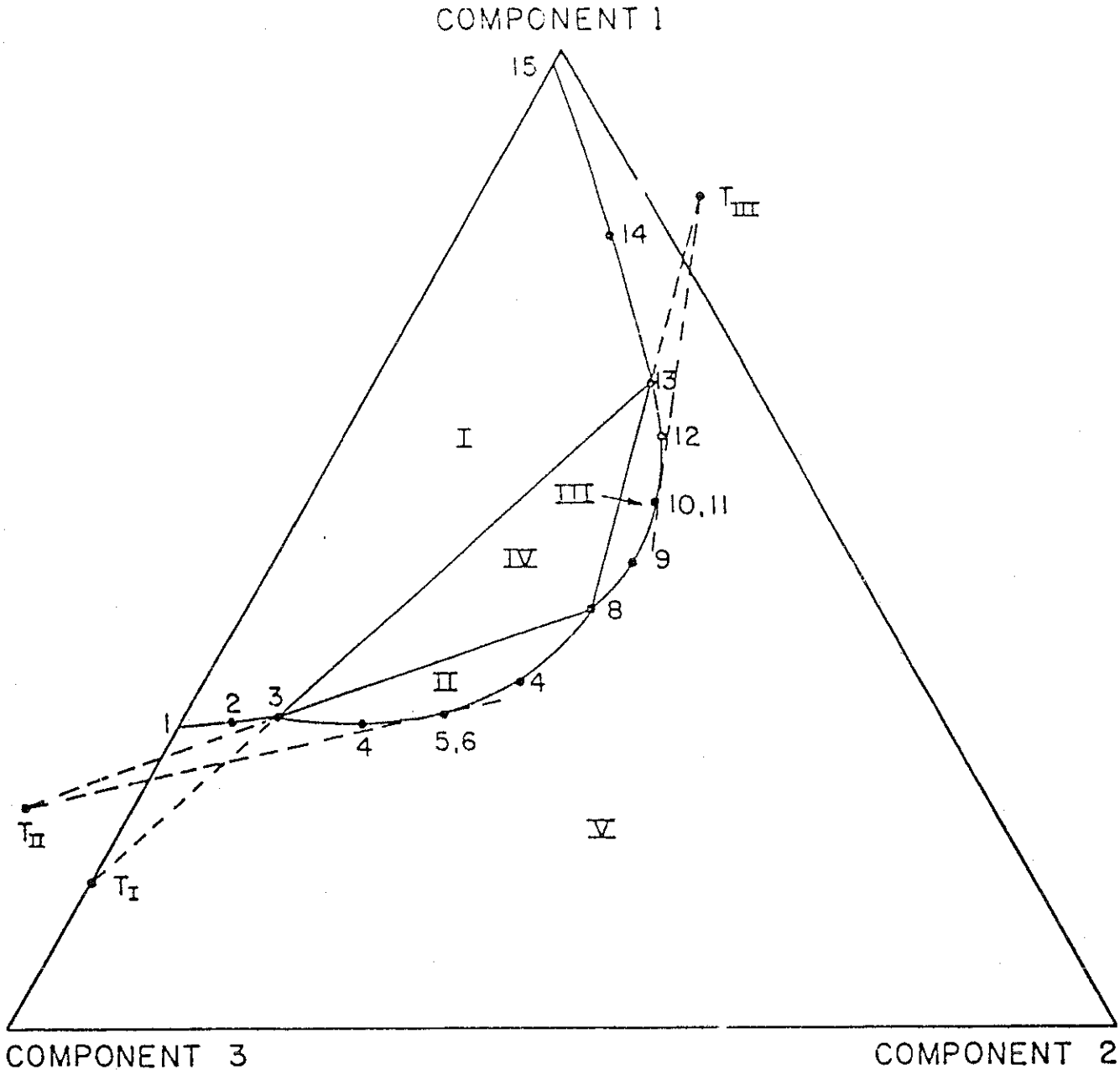

Figure 13 Representation of equilibrium phase behavior of ternary mixtures for one-dimensional simulation of CO_2 flooding. Binodal curves are represented as six pieces of quadratic in the mole fraction of component 1. For instance, the binodal curve for region I is obtained by fitting one quadratic through points 1,2 and 3 for the lower phase and another through points 13, 14 and 15 for the upper phase. Equilibrium tie-lines for each region are assumed to pass through a single point when extended. Point T_I is the tie line intersection point for region I. Overall compositions lying in region IV form three phases with compositions given by points 3, 8 and 13.

Relative permeability curves for water, oil and gas are entered either in the form of a standard table lookup or as

$$k_{rw} = E_w \left(\frac{S_w - S_{wc}}{1 - S_{or} - S_{wc}} \right)^{e_w}$$

$$k_{row} = E_{ow} \left(\frac{1 - S_w - S_{or}}{1 - S_{or} - S_{wc}} \right)^{e_{ow}} \qquad (3)$$

$$k_{rog} = E_{ow} \left(\frac{S_L - S_{Lc}}{1 - S_{Lc}} \right)^{e_{og}}$$

$$k_{rg} = E_g \left(\frac{S_g - S_{gc}}{1 - S_{Lc} - S_{gc}} \right)^{e_g}$$

where k_{rw} = water relative permeability

k_{row} = oil relative permeability (water-oil)

k_{rog} = oil relative permeability (gas-oil)

k_{rg} = gas relative permeability

S_{wc} = irreducible water saturation

S_{or} = residual oil to water

S_{og} = residual oil to gas in the presence of irreducible water saturation

S_{gc} = critical gas saturation

E_w = water relative permeability when oil saturation is S_{or}

E_{ow} = oil relative permeability when water saturation is S_{wc}

E_g = gas relative permeability when the liquid saturation is $S_{wc} + S_{og}$

S_L = liquid saturation, $S_w + S_o$

and $S_{Lc} = S_{wc} + S_{og}$

Values of S_{wc}, S_{or}, S_{og}, S_{gc}, E_w, E_{ow}, E_g and the curve fit exponents e_w, e_{ow}, e_{og}, e_g are specified by the user.

Phase viscosities are calculated from phase compositions by one of two methods. The first is a quarter power blending rule[23]

$$\mu_j = \frac{\mu_1\mu_2\mu_3}{[C_{1j}(\mu_2\mu_3)^{1/4} + C_{2j}(\mu_1\mu_3)^{1/4} + C_{3j}(\mu_1\mu_2)^{1/4}]^4} \quad (4)$$

The second is a two variable table lookup which interpolates a viscosity from the three nearest surrounding data points.

The algorithm used in the fully explicit finite difference calculation is, then:

(1) Given a set of overall volume fractions C_i from initial data or from the previous time step, calculate phase compositions which satisfy the assumption of chemical equilibrium in each grid block.

(2) Calculate fluid properties (density, viscosity) for each phase from phase compositions.

(3) Calculate phase saturations.

(4) Calculate phase relative permeabilities and fractional flows.

(5) Calculate overall volume fractions at the next time level using equation (1).

Numerical Dispersion

The fully explicit backward difference scheme used to solve equation (1) has been analyzed by Lantz.[24] Simultaneous convection and dispersion for a two component system is described by

$$\frac{\delta C}{\delta \tau} + \frac{\delta C}{\delta \xi} - D\frac{\delta^2 C}{\delta \xi^2} = 0 \quad (5)$$

where C is the volume fraction of one component and D is an inverse Peclet number given by

$$D = \frac{\phi A \tilde{D}}{qL} \quad (6)$$

where $\tilde{D}$ is the dispersion coefficient. As shown by Lantz,[2] the numerical diffusivity (numerical dispersion coefficient) for a miscible displacement is

$$D^* = \tfrac{1}{2}(\Delta\xi - \Delta\tau) \quad (7)$$

so that time truncation error can be used to cancel spatial truncation error. If the dimensionless time step $\Delta\tau$ is equal to the grid block size, then there is no numberical contribution to dispersion. If $\Delta\tau$ is greater than $\Delta\xi$, the numerical solutions are unstable. In the model described here, dispersion is included only to the extent that equation (22) or the immiscible analogue described

below can be used to select grid block and time step sizes to produce an appropriate level of numerical dispersion.

When more than one phase is flowing, the local truncation error depends on the nonlinearity of the fractional flow function.[2] For two phase flow (water displacing oil), the numerical diffusivity is

$$D^* = \frac{df_w}{dS_w} \left(\Delta\xi - \frac{df_w}{dS_w} \Delta\tau \right) / 2 \qquad (8)$$

Positive values of D*are required for stable solutions, so the time step limitation will be more severe for immiscible flow than it is for miscible cases if $\frac{df_w}{dS_w} > 1$, as is often true.

In the more complex flow situations simulated here, compositional effects on phase viscosities and three or four phase flow will also have an effect on the level of numerical dispersion. Equations (7) and (8), therefore, should be treated as estimates of the dispersion level rather than quantitative measures. For many applications, however, the savings in computational effort over detailed simulation of dispersion contributions more than justify the somewhat reduced accuracy of the use of numerical dispersion to model physical dispersion.

Simulation of Analogue Displacements

Simulations of runs 1-5 and 7 have been made using the simulator described above. Results of the simulations are shown in Figures 14-23. Density and viscosity data given in Table 1 were used in the simulations. Because alcohol-water mixtures show appreciable hydrogen bonding, viscosities of such mixtures are higher than that of either component, requiring the use of the table lookup option in the simulator. All runs were made with 20 grid blocks and a time step size of .02PV. Relative permeability curves reported by Naar, et al[36] were used without adjustment.

Run 1, shown in Figure 14, was a test of the accuracy of the relative permeability curves for a completely immiscible displacement. Solid curves were computed by the simulator; data points were measured. The sharp decrease in brine production when IC_8 breaks through is characteristic of an immiscible displacement.

In run 2, the bead pack was initially saturated with a mixture of 50 volume percent IPA and 50 volume percent brine. In this run, IPA is recovered more efficiently because it is extracted by IC_8, but the displacement is still essentially immiscible. Ic_8 breakthrough occurs earlier than in run 1 because the IPA-brine mixture being displaced has a higher viscosity than that of brine alone. Calculated and measured recovery curves agree very well, as shown in Figure 15. Calculated and measured values of the overall compositions of produced fluids are plotted in Figure 16. Again, solid curves are computed, data points measured. Three calculated composition paths, for the inlet, middle and outlet grid blocks are plotted, though they differ only slightly. Indeed the paths for blocks 10 and 20 coincide and lie to the right of that for block 1. The overall compositions of fluids flowing out of block 20 should agree with the experimental values of the overall composition of the produced fluids. As Figure 16 demon-

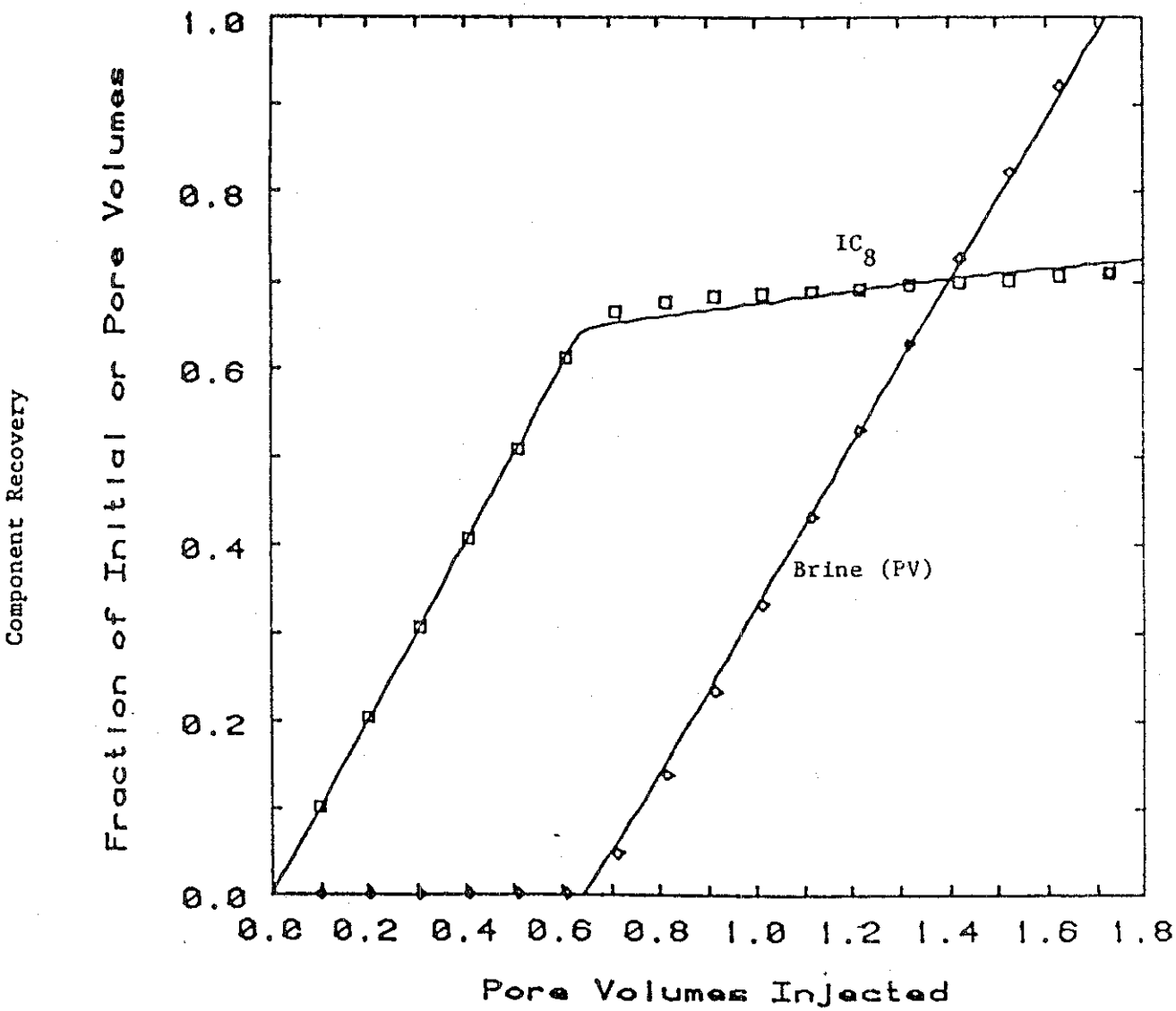

Figure 14 Run 1: Comparison of simulation and experiment for displacement of brine by iso-octane (IC_8). Data points are experimental results. Solid curves are computed results.

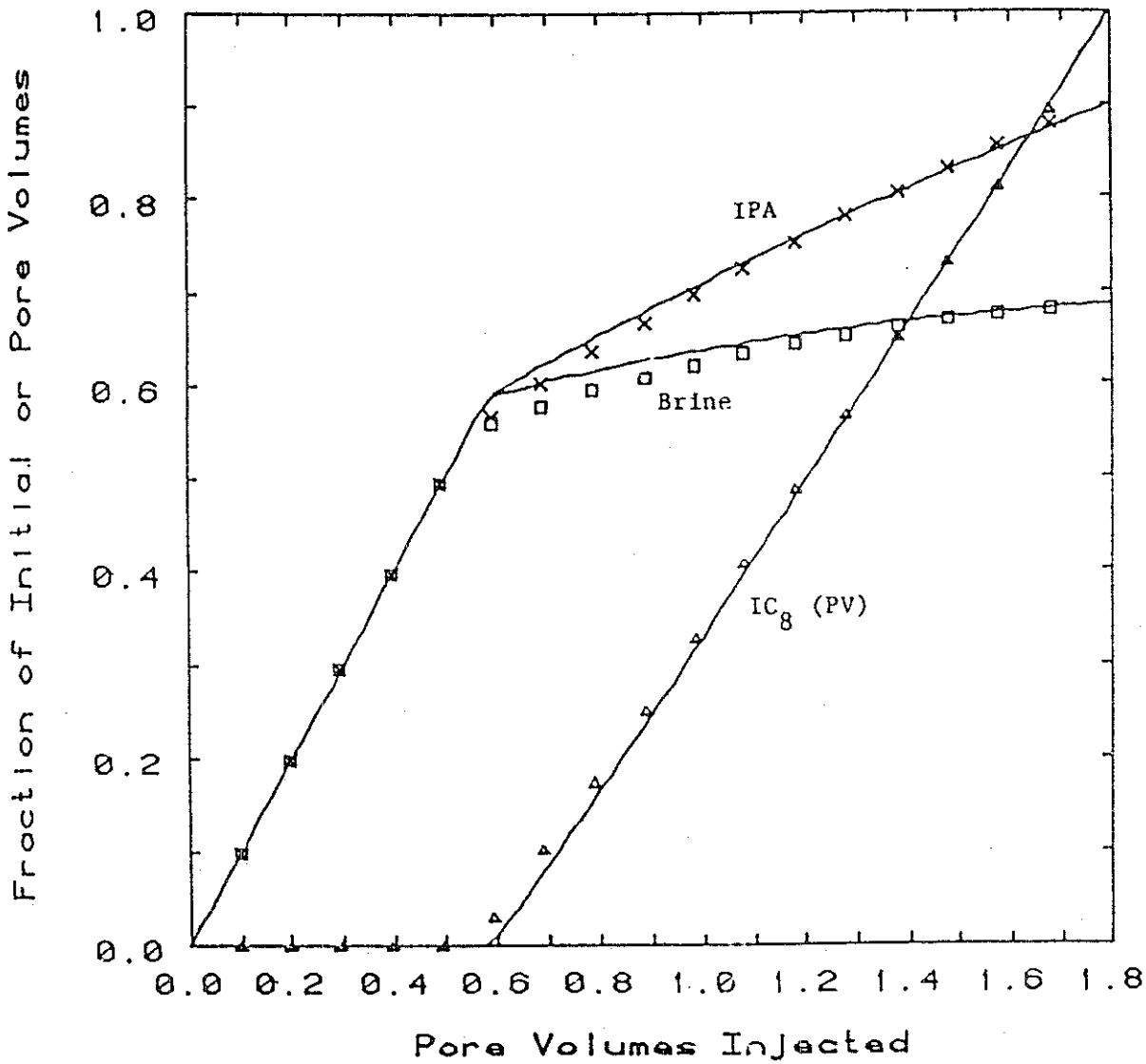

Figure 15. Run 2: Comparison of simulation and experiment for displacement of 50 vol. % iso-propanol (IPA)-50 vol. % brine (2 wt. % $CaCl_2$) by iso-octane (IC_8). Component recoveries for brine and IPA are plotted as fractions of the amount initially present in the bead pack. IC_8 production is in pore volumes (PV).

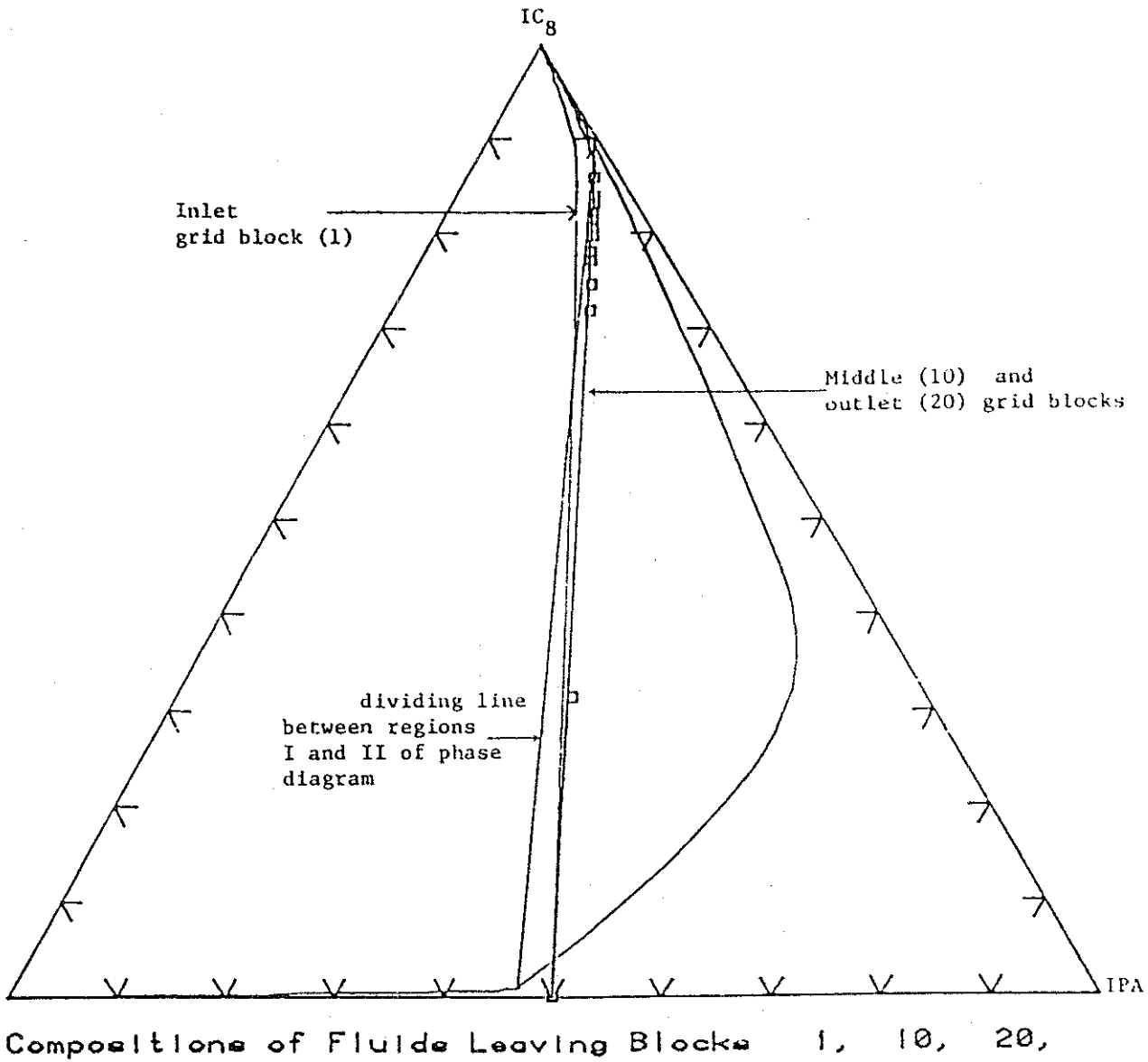

Figure 16 Run 2: Comparison of simulated and experimental values of the overall compositions of produced fluids. Data points are experimental values; solid curves are computed. Calculated compositions of fluids flowing out of blocks 1, (inlet), 10 (middle), and 20(outlet) are plotted but curves for blocks 10 and 20 coincide. Two phase production was ob-

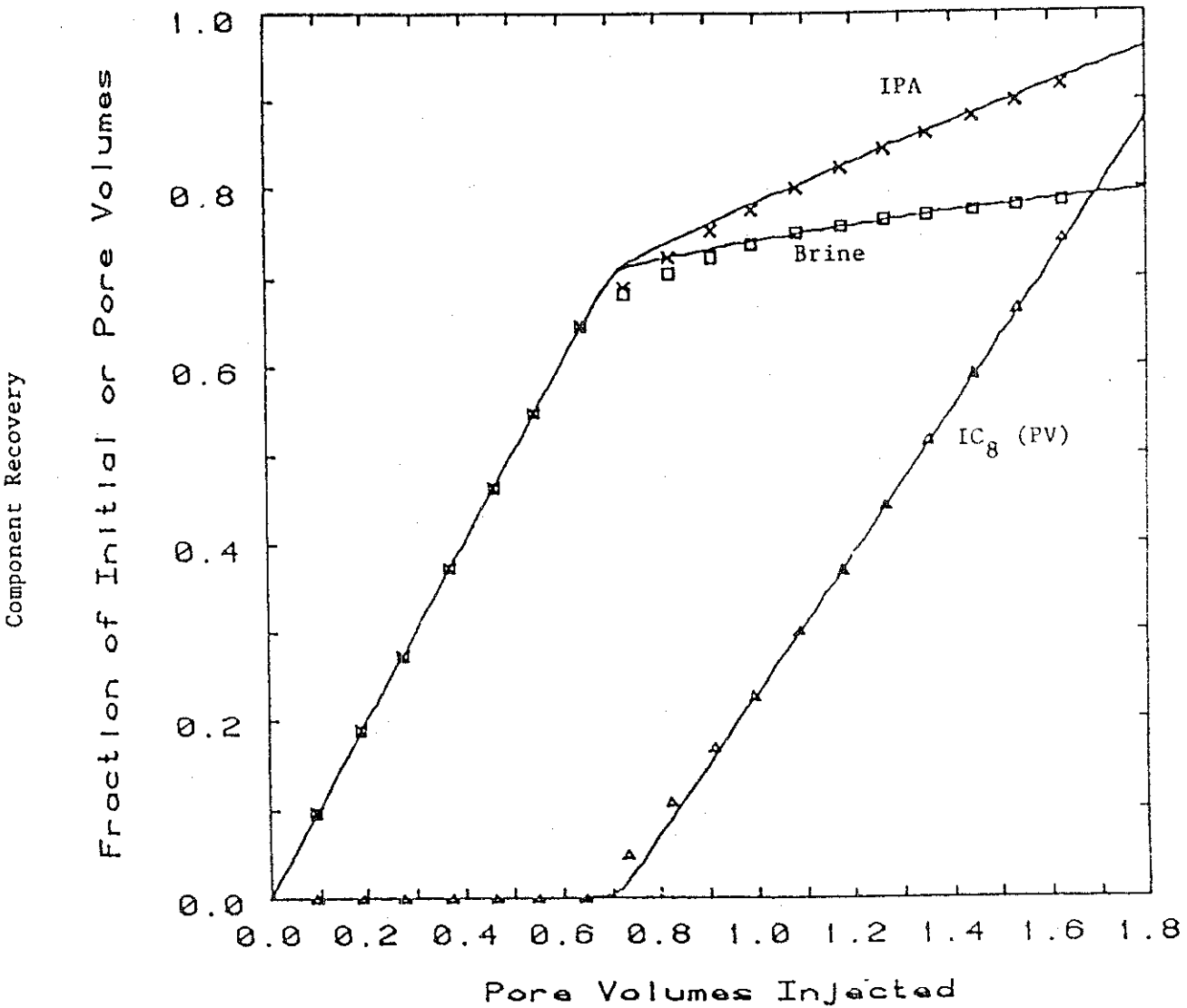

Figure 17 Run 3: Comparison of simulation and experiment for displacement of 75 vol. % iso-propanol (IPA) - 25 vol. % brine (2 wt. % $CaCl_2$) by iso-octane (IC_8). Component recoveries for brine and IPA are plotted as fractions of the amount initially present in the bead pack. IC_8 production is in pore volumes (PV).

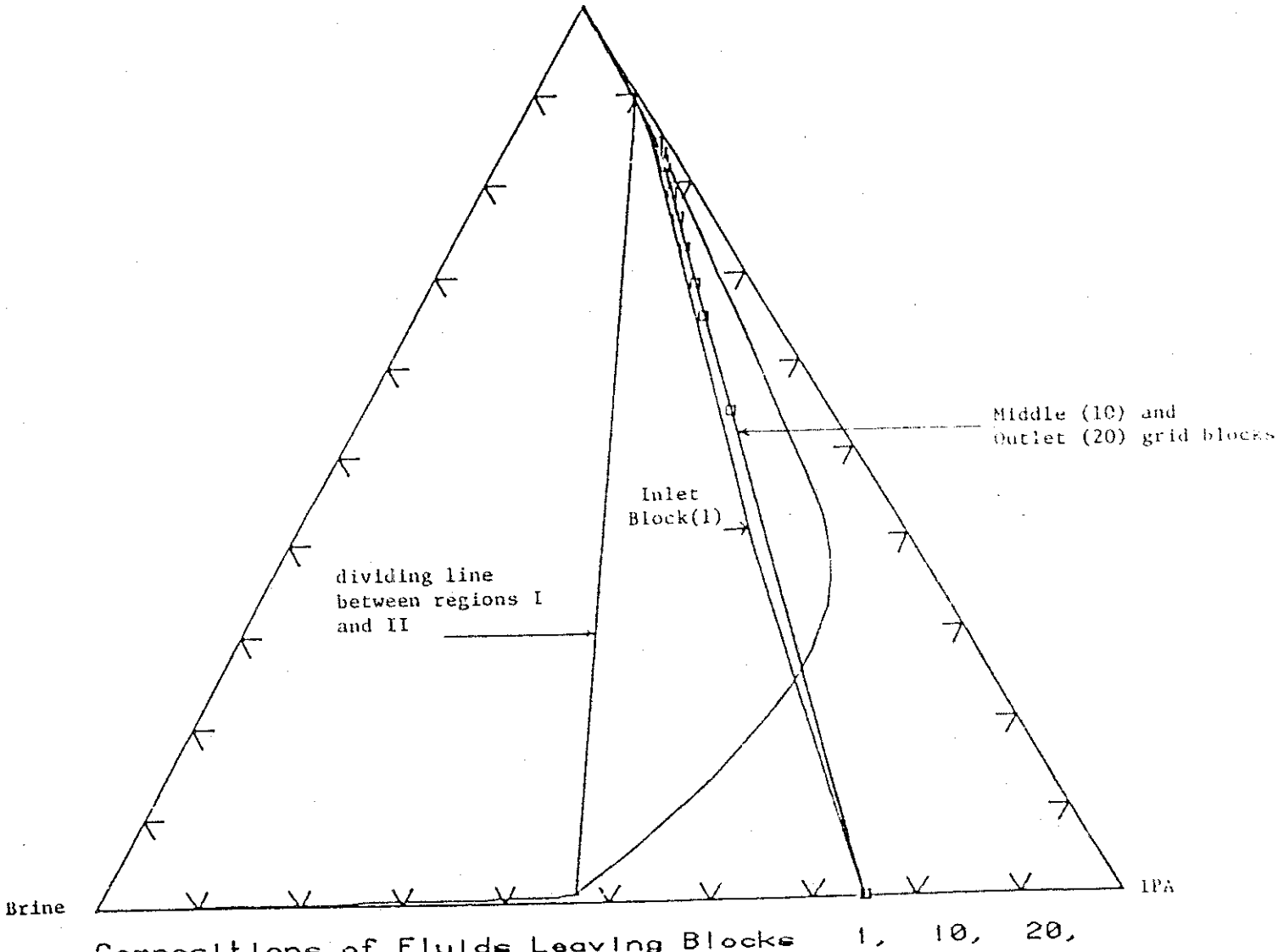

Figure 18 Run 3: Comparison of simulated and experimental values of the overall compositions of produced fluids. Data points are experimental values; solid curves are computed. Calculated compositions of fluids flowing out of blocks 1 (inlet), 10 (middle) and 20 (outlet) are plotted, but curves for blocks 10 and 20 coincide. Two phase production was observed

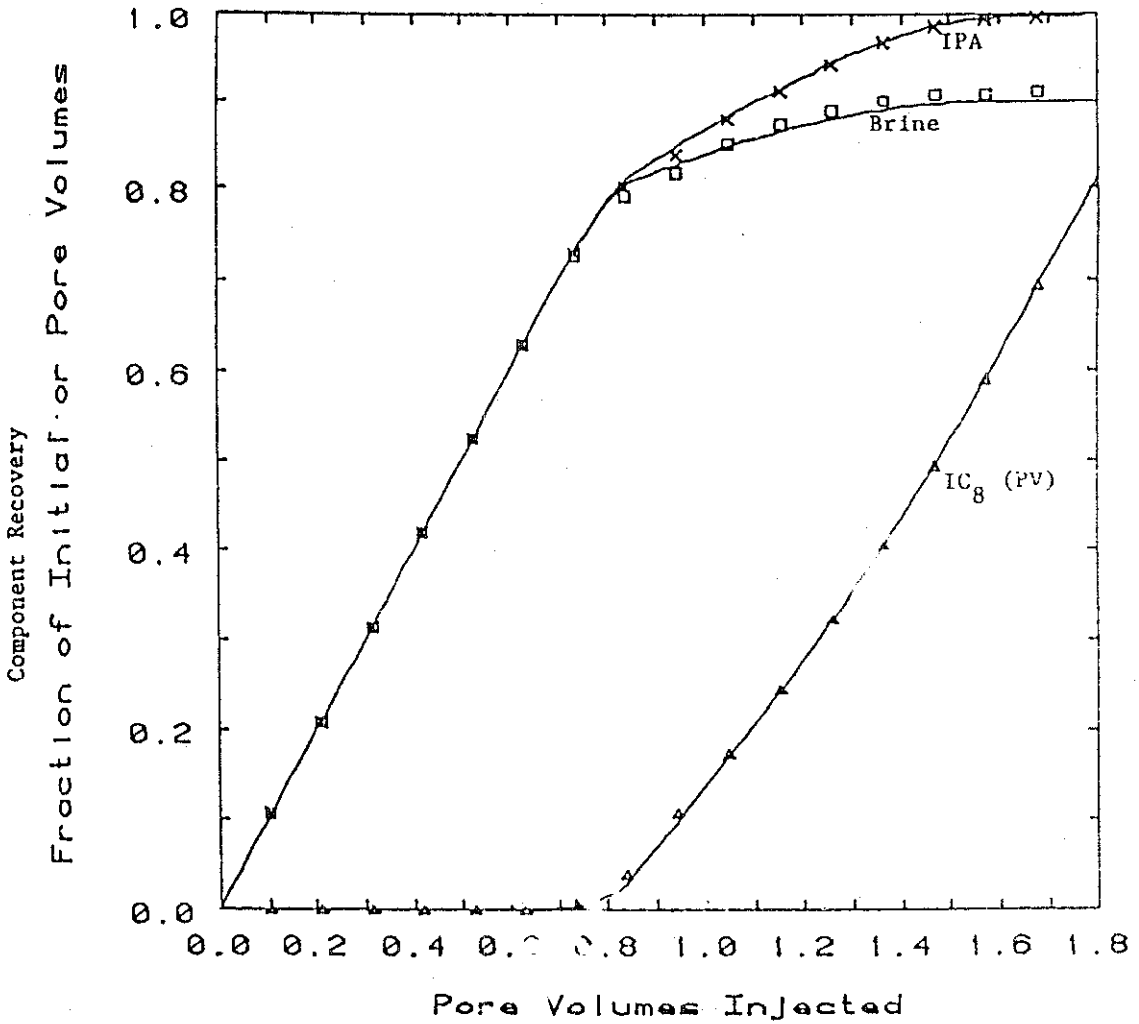

Figure 19 Run 4: Comparison of simulation and experiment for displacement of 85 vol. % isopropanol (IPA)- 15 vol.% brine (2 wt. % $CaCl_2$) by iso-octane (IC_8). Component recoveries for brine and IPA are plotted as fractions of the amount initially present in the bead pack. IC_8 production is in pore volumes. This run developed miscibility during the displacement.

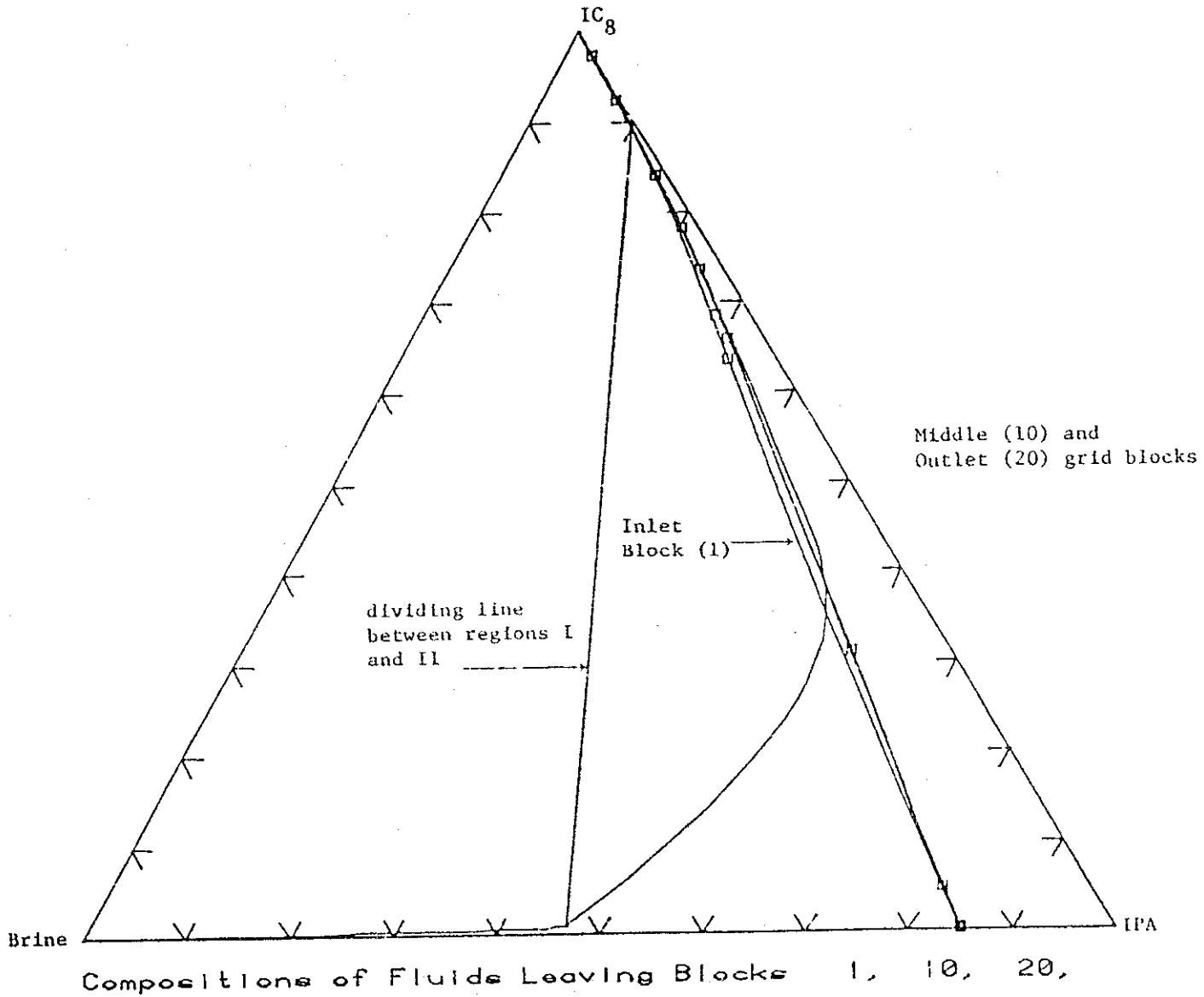

Figure 20. Run 4: Comparison of simulated and experimental values of the overall compositions of produced fluids. Data points are experimental values; solid curves are computed. Calculated compositions of fluids flowing out of blocks 1 (inlet), 10 (middle) and 20 (outlet) are plotted, but surves for blocks 10 and 20 coincide. A short period of two phase flow was observed between 0.84 and 1.25 PV injected, followed by single phase production.

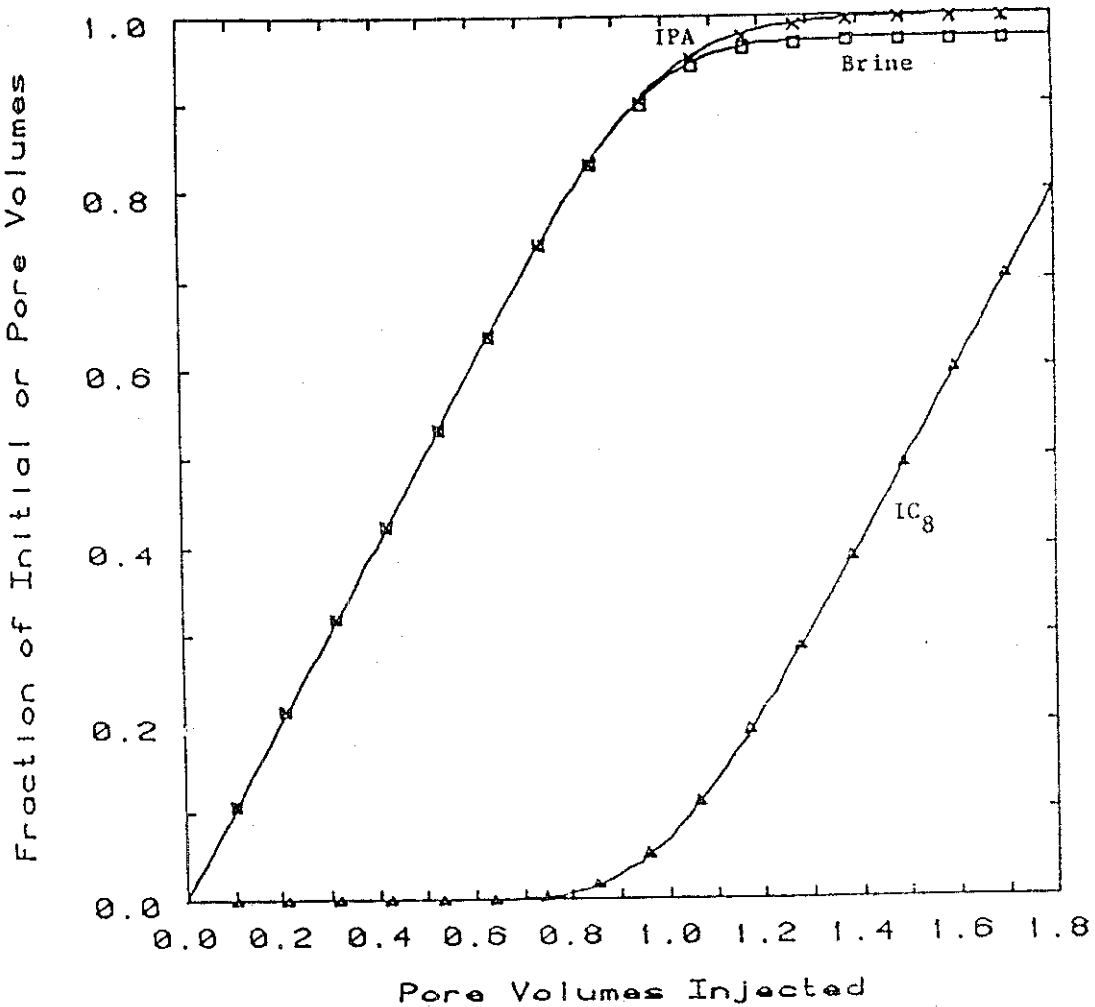

Figure 21. Run 5: Comparison of simulation and experiment for displacement 90 vol.% isopropanol (IPA)--10 vol.% brine (2 wt.%$CaCl_2$) by iso-octane (IC_8). Component recoveries for brine and IPA are plotted as fractions of the amount initially present in the bead pack. IC_8 production is in pore volumes. This run developed miscibility but was nearly first contact miscible.

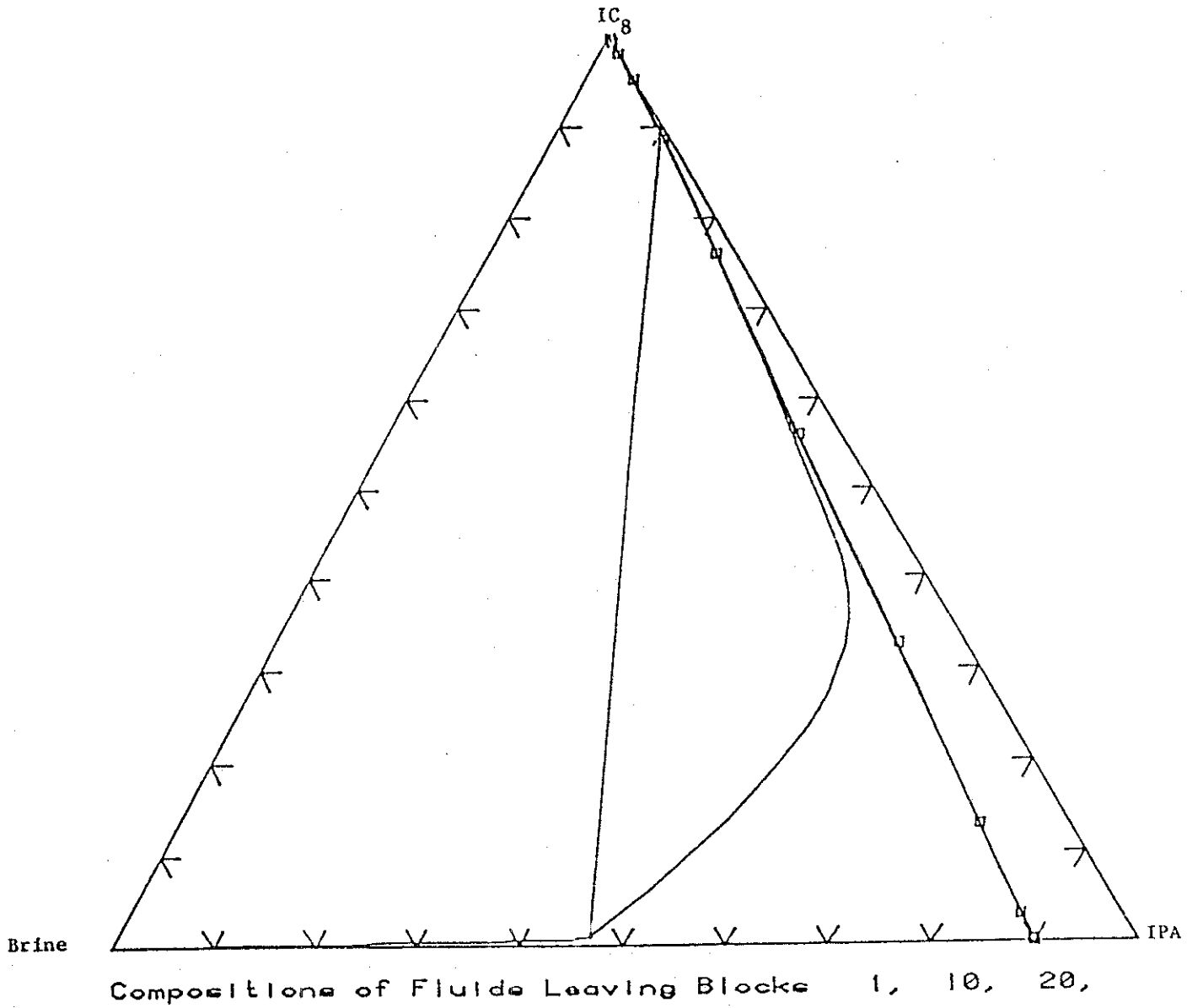

Figure 22. Run 5: Comparison of simulated and experimental values of the overall compositions of produced fluids. Data points are experimental values; solid curves are computed. Calculated compositions, paths of fluids flowing out of blocks 1, 10 and 20 are all identical.

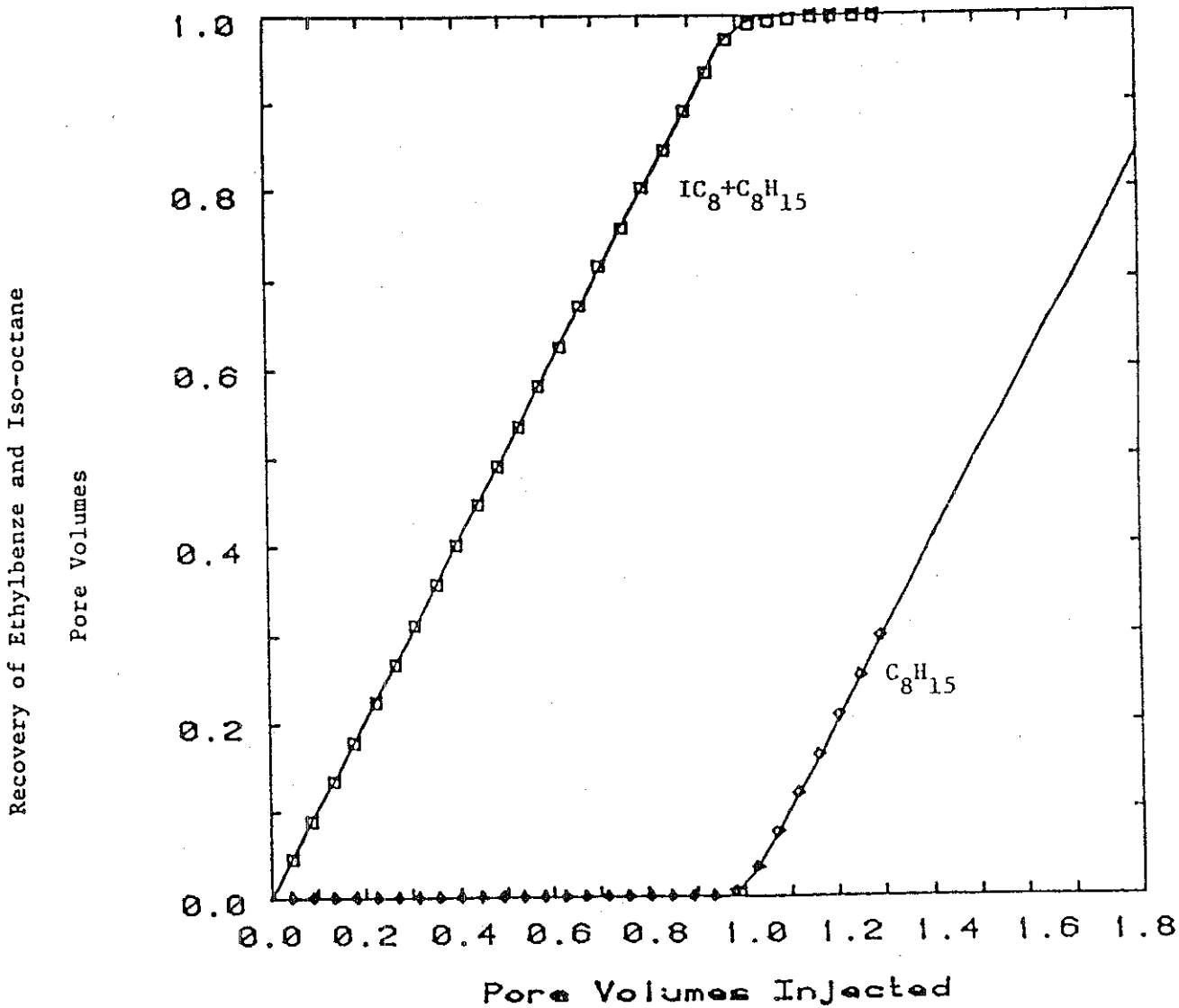

Figure 23 Run 6: Comparison of simulation and experiment for a miscible displacement of 95 vol.% ethylbenzene-5 vol.% iso-octane by ethylbenzene. Curves plotted are pore volumes produced of the mixture initially present and pore volumes of pure ethylbenzene.

strates, the agreement is excellent.

Run 3 was also an immiscible displacement of 75 vol. % IPA - 25 vol.% brine by IC_8. Stripping of IPA is more efficient than i Run 2 but the composition paths change only slightly during the displacement indicating that little enrichment of the upper phase is occurring. Two phase production was observed from breakthrough (0.68 PV) to 1.17 PV injected, after which only a single phase containing mainly IC_8 and IPA was produced. Excellent agreement between calculated and experimental results is shown in Figures 17 and 18 for run 3.

Run 4, results of which are shown in Figures 19 and 20, was on the borderline of developing miscibility, and the recovery curves show the slower drop in IPA and brine production after IC_8 breakthrough that is characteristic of miscible displacements. A short period of two phase production (between 0.84 and 1.25 PV injected), the result of dispersion, was observed. Run 5 (Figures 21 and 22) was very nearly a first contact miscible displacement for which the recovery was correspondingly high. Only a very small amount of extraction of IPA by IC_8 is required to develop miscibility. Accordingly, recoveries of IPA and brine are nearly the same, and the displacement is very efficient. Single phase production was observed throughout the run.

Figure 23 shows results of a displacement of a mixture of IC_8 and ethylbenzene by pure ethylbenzene. This experiment was used to determine the dispersion coefficient for the bead pack. The dispersion coefficient was determined to be 3.12×10^{-4} cm^2/sec which agrees closely with values given by Blackwell.[37] It should be noted, however, that the levels of numerical dispersion required to give a good match of experimental with calculated results for runs where two phase flow results as an order of magnitude higher than that used to match the miscible displacement. Reasons for this behavior will be discussed in detail in a later report.

The excellent agreement obtained between experimental and simulated displacements suggests that the one dimensional simulator developed here, with accurate input data for phase behavior, fluid properties and dispersion, can be used to build understanding of the physical mechanisms important in the displacement process. Extensions to more complex phase behavior and more complex porous media are underway.

Task 4. Application of Laboratory Results to Field Problems

Much of the work to be done under this task must wait until the laboratory experimental work is more complete, but research has begun in two areas which have direct impact on the translation of laboratory results to predictions of field performance, and on the development of recommendations for a suite of laboratory experimental evaluations for a particular field application. First, the representation of a crude oil as a small number of pseudo-components is being explored. Any field scale prediction of CO_2 flood performance will require numerical simulation, but field scale compositional simulations of the process are impractical if a large number of components (e.g. as used by Fussell[11]) are required to calculate phase behavior of CO_2-crude oil mixtures. Thus, the use of a small number of pseudo-components should be evaluated and may be required if practical simulations are to succeed. Characterization of crude oils by gas chromatography, probably in combination with a simple distillation to characterize heavy ends, will provide essential data for this effort, and be coupled with phase behavior computations using the two equations of state[13,25] programs on hand.

Analysis of CO_2-Crude Oil Phase Diagrams

The second area is an analysis and comparison of the phase behavior of CO_2-crude oil mixtures with that of mixtures of CO_2 and well-characterized hydrocarbons. The purpose of this analysis is to develop a qualitative understanding of the differences between observed phase behavior for low temperature (<50°C) and high temperature CO_2-crude oil systems, with the eventual aim of relating equilibrium phase behavior, observed in static experiments to the dynamics of the displacement process.

Binary CO_2-crude oil phase behavior experiments have produced two distinct types of phase envelopes as shown in Figures 24 and 25. At temperatures above about 50°C (122°F), binary mixtures of crude oils and CO_2 show liquid-vapor separations (along with possible precipitation of a solid phase).[6,10] At low CO_2 concentrations, reduction of the pressure of the mixture from a high level produces a vapor phase when the mixture reaches the bubble point pressure (curve B, Figure 24). At high CO_2 concentrations, very high pressures are required to maintain the mixture as a single phase. Pressure reduction causes the mixture to pass through a dew point (curve D) where a small amount of liquid forms. Further reductions in pressure cause the liquid volume to grow with retrograde vaporization occurring at still lower pressures. The bubble point and dew point curves meet at a critical point C. Phase diagrams of this sort have been reported by Simon *et al*,[6] Perry *et al*[2,7] Graue and Zana,[26] and Rathmell *et al*.[5]

Phase behavior is significantly more complex for CO_2-crude oil mixtures at temperatures below about 50°C[1,7,10,28] (see Figure 25). Bubble points are observed at CO_2 concentrations below about 60 mole percent (curve B). At higher CO_2 concentrations, liquid-liquid equilibria occur. Two liquid phases occur at pressures and compositions within the region bounded by the curve labeled LL and B, an upper phase presumably rich in CO_2, and a lower phase rich in the heavier hydrocarbons from the crude oil. As the pressure is reduced, a vapor phase appears in addition to the two liquid phases when the curve B is crossed. When the curve D is reached, the upper liquid phase has disappeared leaving only liquid and vapor.

The complex phase behavior shown in Figure 25 can be understood by examining the behavior of mixtures of CO_2 and normal alkanes. Binary mixtures of CO_2 with normal alkanes lighter than tridecane (C_{13}) exhibit liquid-liquid separations at temperatures below the critical temperature of CO_2 (31°C).[29] For alkanes C_{14} and heavier, the liquid-liquid region extends to temperatures above the critical temperature of CO_2. That is, a binary mixture of CO_2 and hexadecane (C_{16}), say, at 32°C, can exist as a liquid-vapor (L-V) mixture at low pressure, as a liquid-liquid-vapor (L_1-L_2-V) mixture at one higher pressure, and as a liquid-liquid (L_1-L_2) mixture at still higher pressures.[30] At somewhat higher temperatures (above the L_2-V critical temperature), the mixture will pass from an L-V state at low pressures to an L_1-L_2 (or L_1-dense phase) without showing an L_1-L_2-V separation. As the molecular weight of the alkane increases, the maximum temperature at which liquid-liquid separations are observed also increases as Liphard and Schneider's data for CO_2-squalane mixtures clearly indicate.[31] Thus, it is apparent that the appearance of L_1-L_2 and L_1-L_2-V separations in CO_2-crude oil mixtures is strongly related to the system temperature (Huang and Trächt report data which confirm this conjecture),[7]

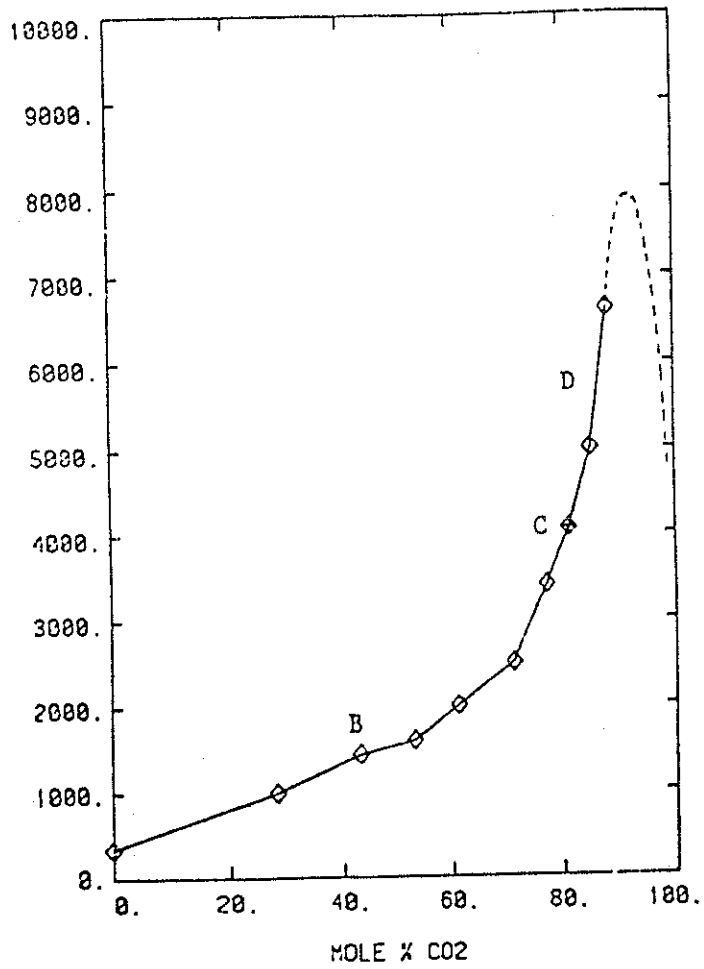

Figure 24 Phase behavior of carbon dioxide and Rangely crude oil at 160°F, after Grave and Zana.[26]

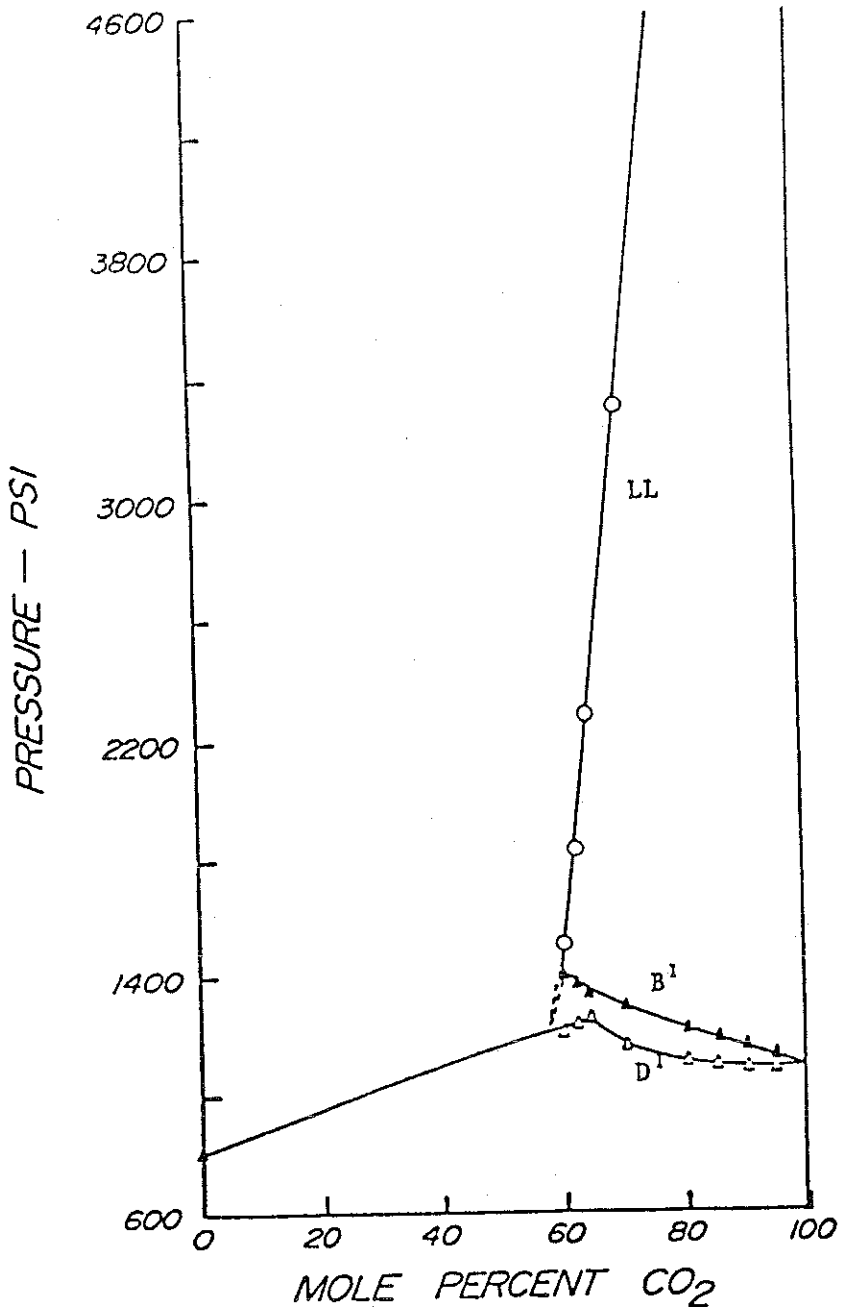

Figure 25. Phase behavior of carbon dioxide and a West Texas crude oil at 94°F, after Shelton and Yarborough.[10]

but the maximum temperature at which such separations occur depends on the crude oil composition. The exact nature of that dependence is not known, but it is likely that increasing the average size of the molecules in the crude oil would increase the maximum temperature for liquid-liquid separations.

Phase behavior studies by Meldrum and Nielsen[32] showed that L_1-L_2-V separations occur for the ternary systems CO_2-C_3-C_{16} and CO_2-C_{10}-C_{16}. Figure 26 shows Meldrum and Nielsen's data for the latter system at 70°F. Three phase separations (L_1-L_2-V) occur at pressures near the pressure at which liquid-liquid separations occur for the CO_2-C_{16} binary. Those data suggest that L_1-L_2-V separations occur when system temperatures and pressures are such that mixtures of CO_2 and the light hydrocarbon components show L-V equilibria and mixtures of CO_2 and heavy components show L_1-L_2 separations.

Interpretation of the phase diagram shown in Figure 25 requires an understanding of the appearance and disappearance of the three phase region as system pressure is increased. Meldrum and Nielsen's[32] experiments provide some information but did not examine in detail the pressure range at which the three phase region appears. Elgin and Weinstock[33] investigated ternary mixtures of ethylene, water, and solvents which exhibit qualitatively similar phase diagrams. Their work suggests that in a ternary system, the three phase region appears with a split in a tie line. With increasing pressure, the invariant phase compositions move as shown schematically in Figure 27, with the three phase region disappearing when the middle phase invariant point reaches the upper phase invariant point. The picture shown in Figure 27 must be treated as qualitative and speculative. In real systems, all three invariant points move as conditions change and much work remains to show that CO_2 crude oil systems behave similarly. Furthermore, while a three phase region must appear or disappear with a split in a tie line, it is not known whether the motion of invariant points always follow the sequence shown in Figure 27 or whether other possibilities exist. Work continues to understand the behavior of these three phase systems. Nevertheless, the qualitative picture shown in Figure 27 is remarkably successful in explaining the behavior observed for CO_2-crude oil systems, as is shown below.

Figure 28 shows hypothetical sequence of ternary phase diagrams for a CO_2-crude oil mixture and Figure 29 shows the pressure-composition (P-X) diagram which results. The crude oil is treated as a mixture of light and heavy pseudo components (50 mole percent each), so that binary mixtures of CO_2 with the oil fall on the vertical line shown in each diagram. At pressure P_1, the mixture shows a bubble point. At P_2, the three phase region has appeared, but is observed only at very high CO_2 concentrations. At P_3, as CO_2 is added to the mixture, it shows first a bubble point and then passes into the three phase region and then back into the two phase region at high CO_2 concentration. At P_4, the middle phase invariant point has passed the binary mixture composition, so that with added CO_2 a liquid-liquid occurs first, followed by the appearance of a vapor phase. Similar behavior occurs at P_5, but the shift in the invariant points at the vertices of the three phase region causes the three phase region to appear at CO_2 concentrations between those observed at P_4. At P_6, the three phase region has disappeared leaving only L_1-L_2 separations.

The phase diagram shown in Figure 29 is similar to that shown in Figure 25 though there are some differences in the order in which phases appear with CO_2 addition. Work continues to develop a sequence of phase diagrams which is completely consistent, therefore, with the type of phase behavior observed for CO_2-crude oil systems at the low temperatures typical of West Texas and New Mexico oil fields. It should be noted, however, that very few experimental

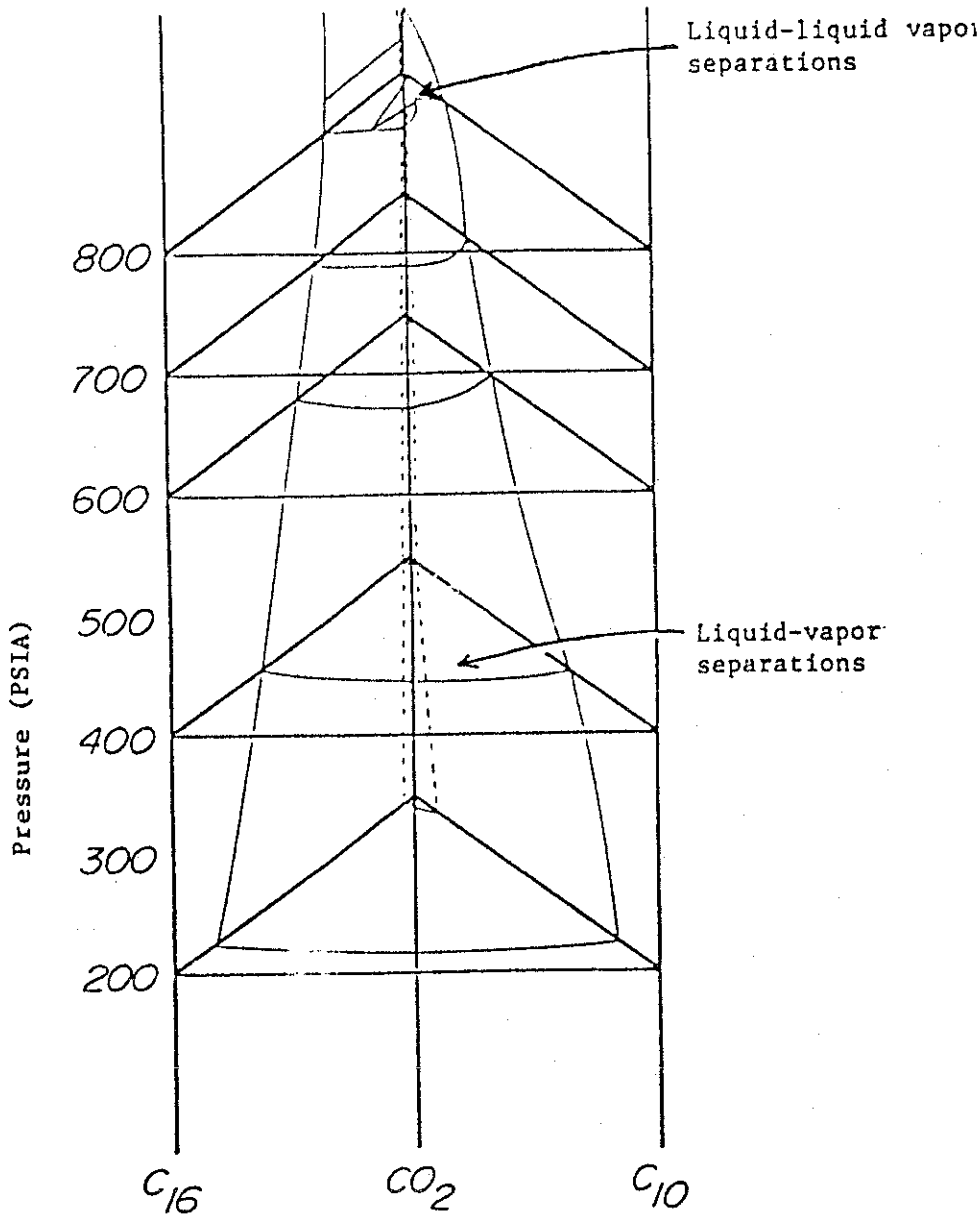

Figure 26. Phase behavior of the ternary system carbon dioxide (CO_2) - decane (C_{10}) - hexadecane (C_{16}). At 800 psia, liquid-liquid-vapor separations occur.

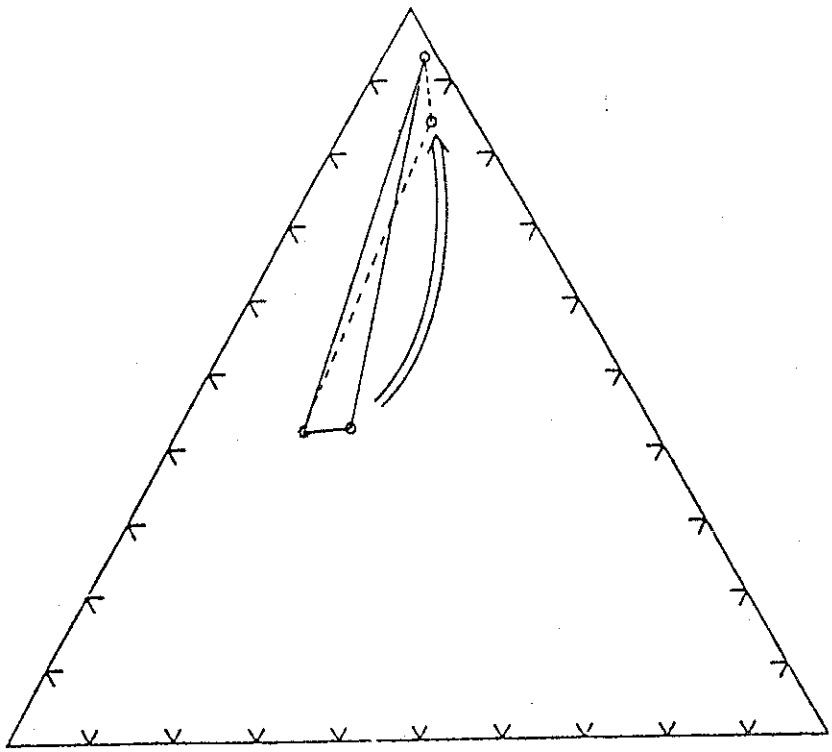

Figure 27. Appearance and disappearance of a three phase region in a ternary diagram. A tie line splits and with increasing pressure one invariant migrates toward another. The three phase region disappears when the migrating invariant point reaches the upper phase invarient point, the inverse of tie line splitting.

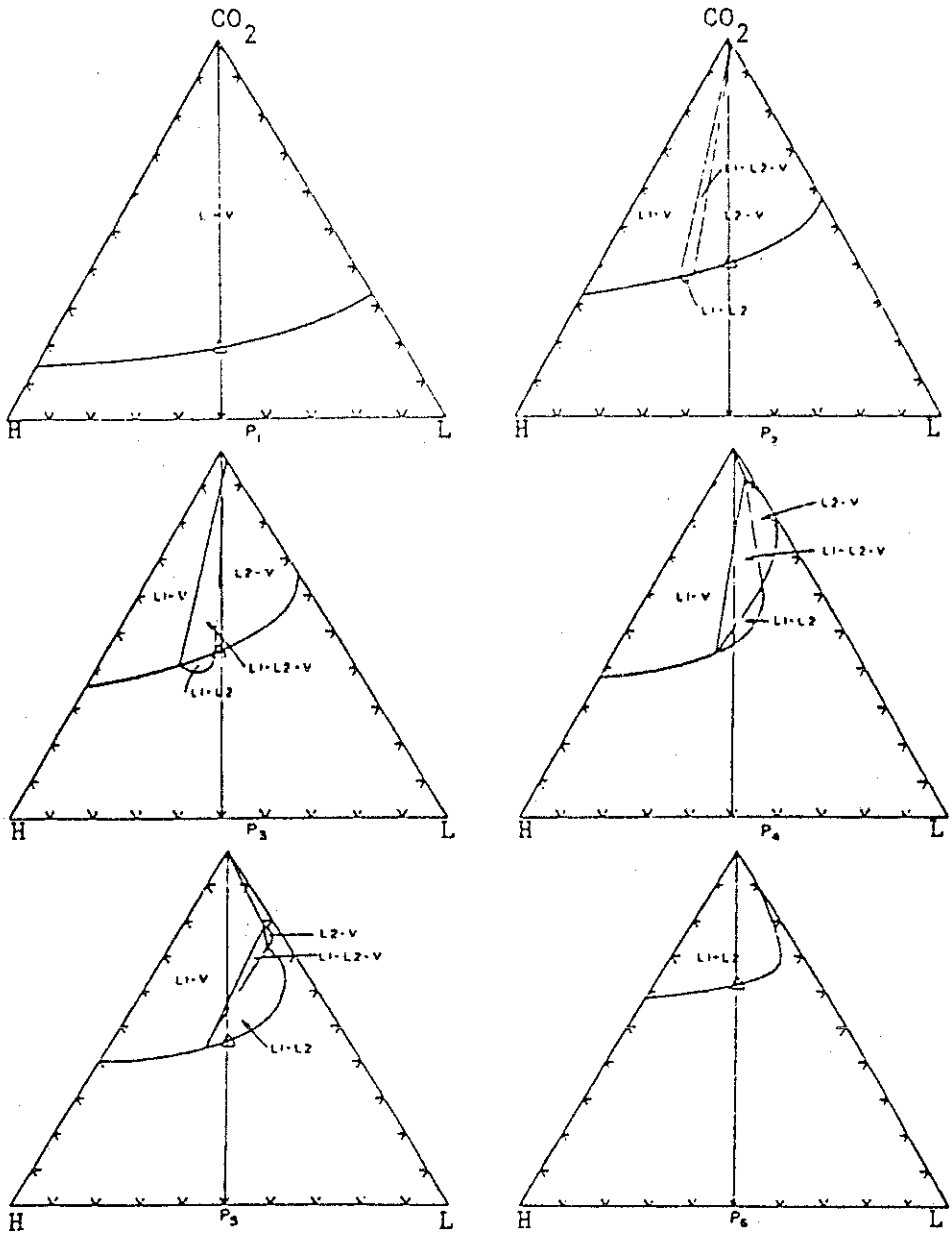

Figure 28. Hypothetical sequence of phase diagrams as pressure increases for CO_2-crude oil mixtures. The oil is represented as 50 mole% each of light (L) and heavy (H) components. Binary mixtures of CO_2 and oil fall on the straight line connecting the CO_2 vertex with the oil composition.

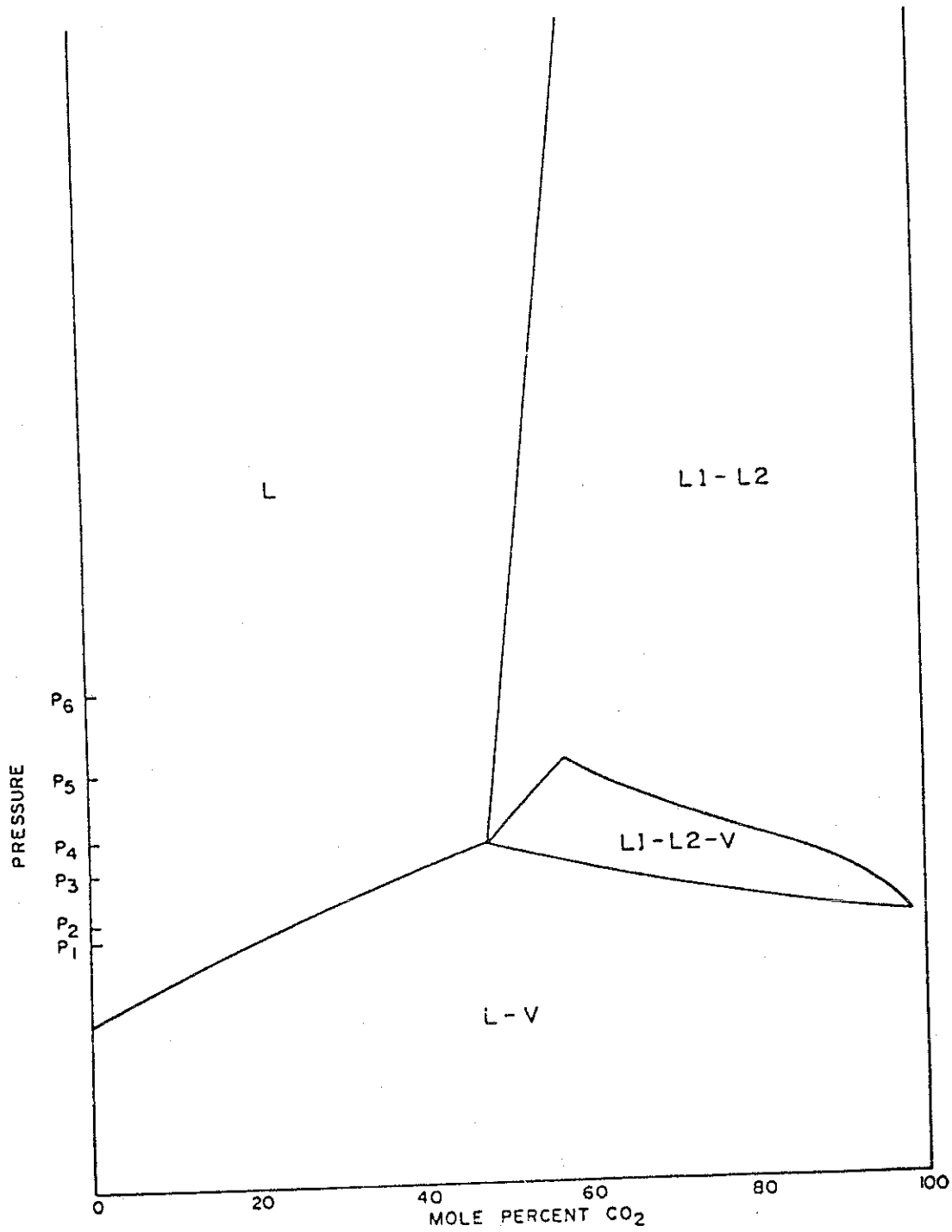

Figure 29 Binary pressure-composition diagram for the hypothetical sequence of phase diagrams shown in Figure 28.

data are available to confirm or deny the phase diagrams hypothesized. The multiple contact experiments planned will provide experimental verification of the analysis presented here.

Effect of Phase Behavior on Displacement Efficiency

The impact of the phase behavior shown on the displacement process can be assessed using the one dimensional simulator described under task 3. Figure 30 shows a hypothetical sequence of phase diagrams for a CO_2-crude oil system. Note that the oil is treated as two pseudo-components, C_1-C_{10} and C_{10}+ and the oil contains approximately 50 mole percent of each component. The binary P-X diagram which results from the sequence of ternary diagrams is shown in Figure 31, and the diagrams of Figures 30 and 31 are combined in a three dimensional pressure-composition diagram in Figure 32.

Secondary displacements of the oil by continuous injection of CO_2 were simulated for each of the pressures shown in Figure 30. Fluid properties and run conditions used for the runs are summarized in Table 3. To isolate the effect of phase behavior, fluid properties were held constant for the four runs; only the phase behavior was changed.

Results of the simulations are shown in Figures 33 and 34. Figure 33 shows recovery curves for each of the cases, while Figure 34 shows overall composition paths for the middle and outlet grid blocks. The displacement efficiency increases dramatically with pressure, as shown by the recovery curves (Figure 32). At 1000 psi, CO_2 breakthrough occurs at 0.35 PV injected, there is no difference in the amounts of C_1-C_{10} and C_{10}+ recovered, and oil production drops rapidly after CO_2 breakthrough. At 1200 psi, breakthrough is delayed to 0.60 PV and the recovery at 1 PV injected is correspondingly higher. The amount of C_1-C_{10} recovered exceeds that of C_{10}+ because CO_2 extracts C_1-C_{10} more efficiently at this pressure. At 1300 psi, recovery has improved further, with breakthrough delayed to 0.8 PV. The displacement at 1400 psi shows little additional improvement in recovery, indicating that an experimentally determined miscibility pressure would be near 1300 psi. The recovery results are summarized in Figure 35, which reports breakthrough recovery and recovery at 1 PV injected for each pressure.

The reason for the improvement in recovery as pressure increases lies in the efficiency of the extraction of C_1-C_{10} by CO_2, as is shown in composition path diagrams shown in Figure 3. In each case the overall composition, a linear combination of the compositions of all phases present, changes from the initial oil composition to high CO_2 concentrations as the run progresses. At 1000 psi, the overall composition in each block traverses the tie line which, when extended, passes through the oil composition. No enrichment of the more mobile CO_2 rich phase occurs. At 1200 psi, the three phase region has appeared, but the phase diagram is still dominated by tie lines of the two phase region which extend to the oil composition. The displacement is more efficient, however, because the extraction is more efficient than at 1000 psi, so that some enrichment of the CO_2 by C_1-C_{10} occurs. At 1300 psi, the alteration in the shape of the three phase triangle has produced a diagram dominated by the strong extraction of the liquid-liquid region. The composition path clearly shows the enrichment of the overall compositions in the middle and outlet grid blocks. Note that there is little difference between the paths of the two grid blocks indicating that the

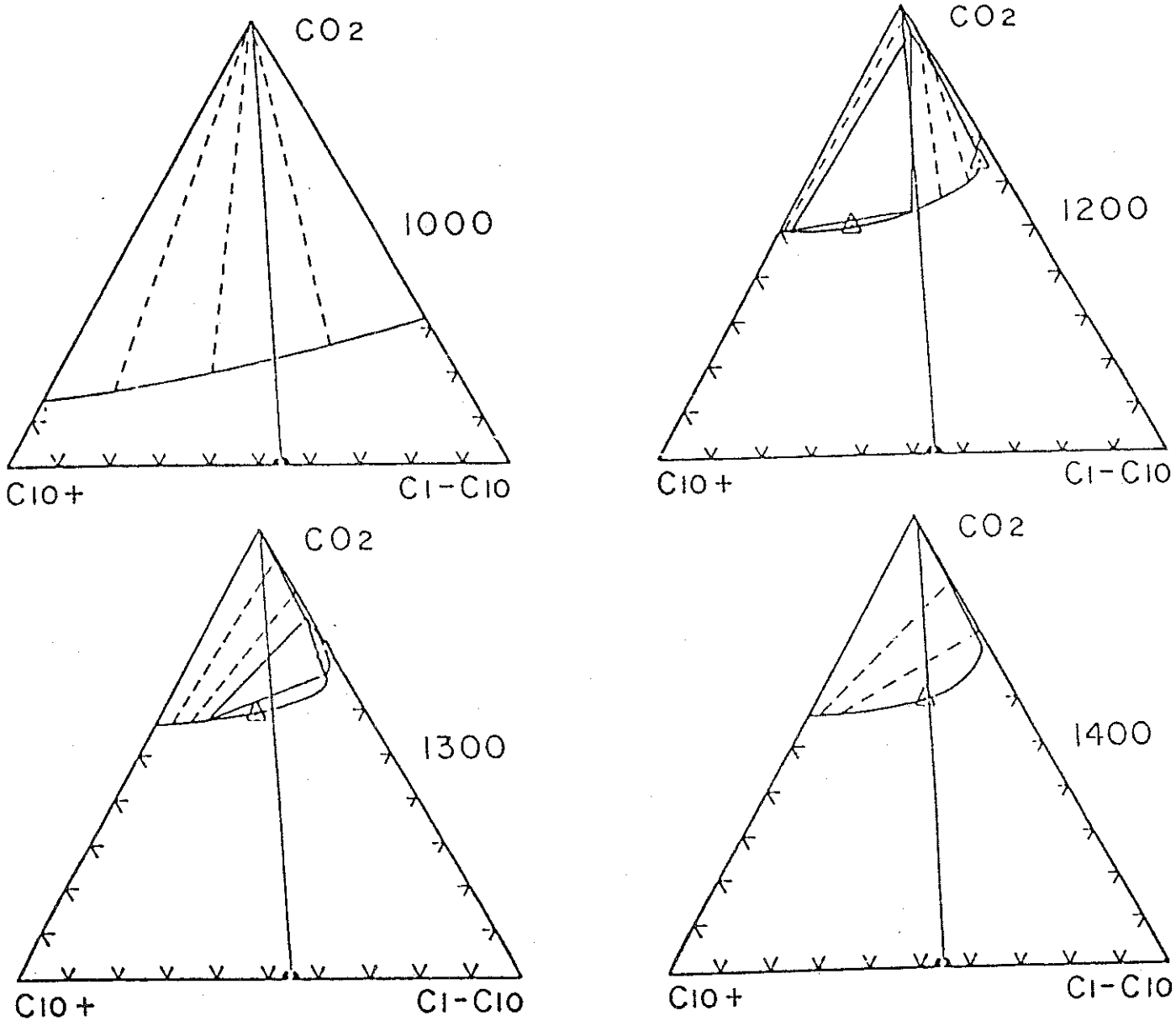

Figure 30 Phase diagrams for a hypothetical CO_2-oil mixture at four pressures.

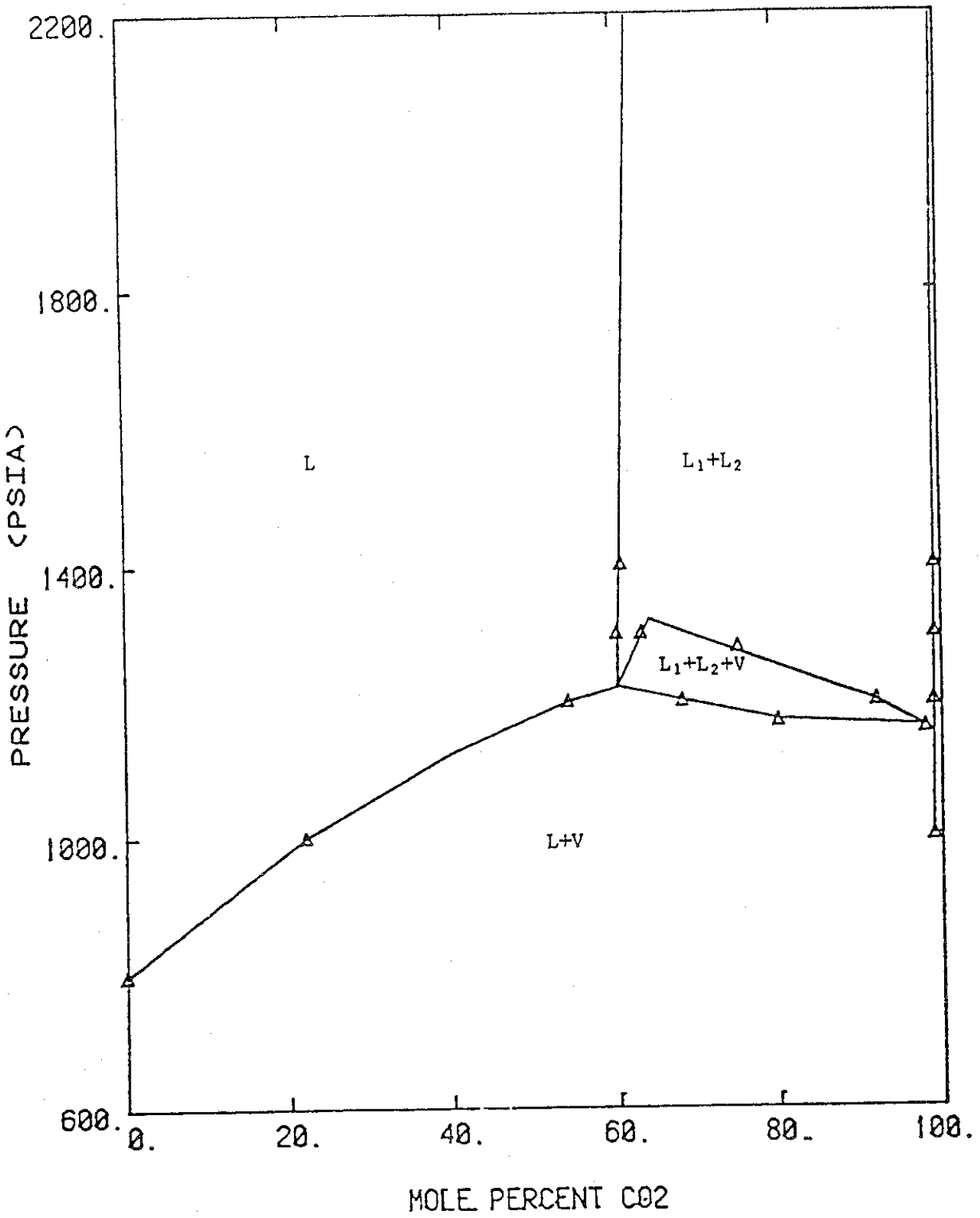

Figure 31 Binary pressure-composition diagram for the CO_2-oil system shown in Figure 30.

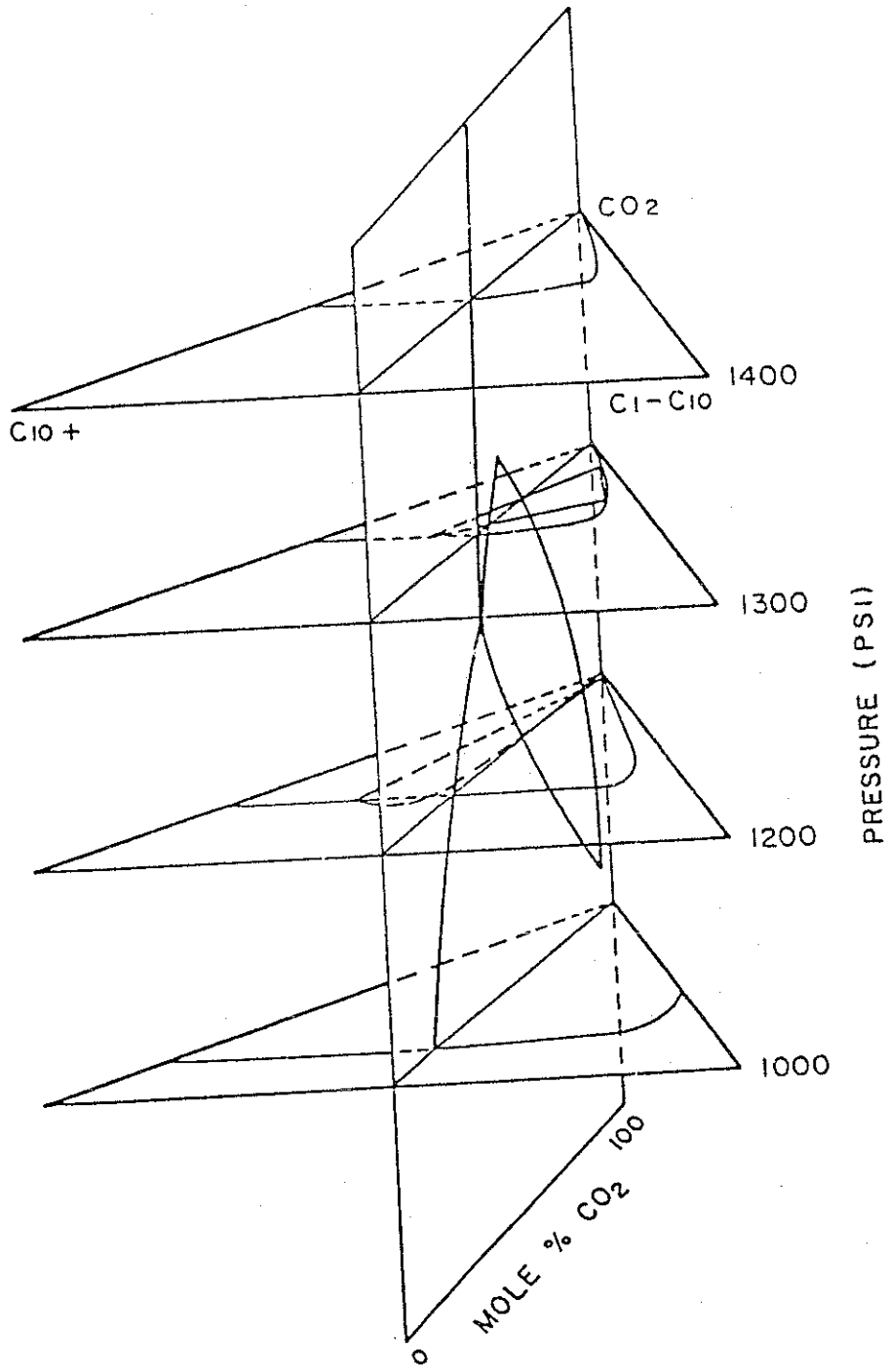

Figure 32. Combined pressure-composition and ternary diagrams for the hypothetical CO_2-oil system shown in Figure 30.

Table 3. Fluid Properties and Run Conditions for Simulation of Displacement of Crude Oil by CO_2

Number of grid blocks 40

Time step size .005 PV

Component	Viscosity (cp)	Density (g/cm^3)	Mole Weight
CO_2	.04	.65	44
C_1-C_{10}	.50	.65	64
C_{10+}	2.00	.90	276
H_2O	1.00	1.00	18

Relative Permeability Data

$S_{wc} = 0.200$	$E_w = 1.$	$e_w = 2.$
$S_{or} = 0.400$	$E_{ow} = 1.$	$e_{ow} = 2.$
$S_{og} = 0.400$	$E_g = 1.$	$e_{og} = 2.$
$S_{gc} = 0.$		$e_g = 2$

Initial Oil Composition (Mole Fractions)

Component	Mole Fraction
CO_2	0
$C_1 - C_{10}$	.5446
C_{10+}	.4554

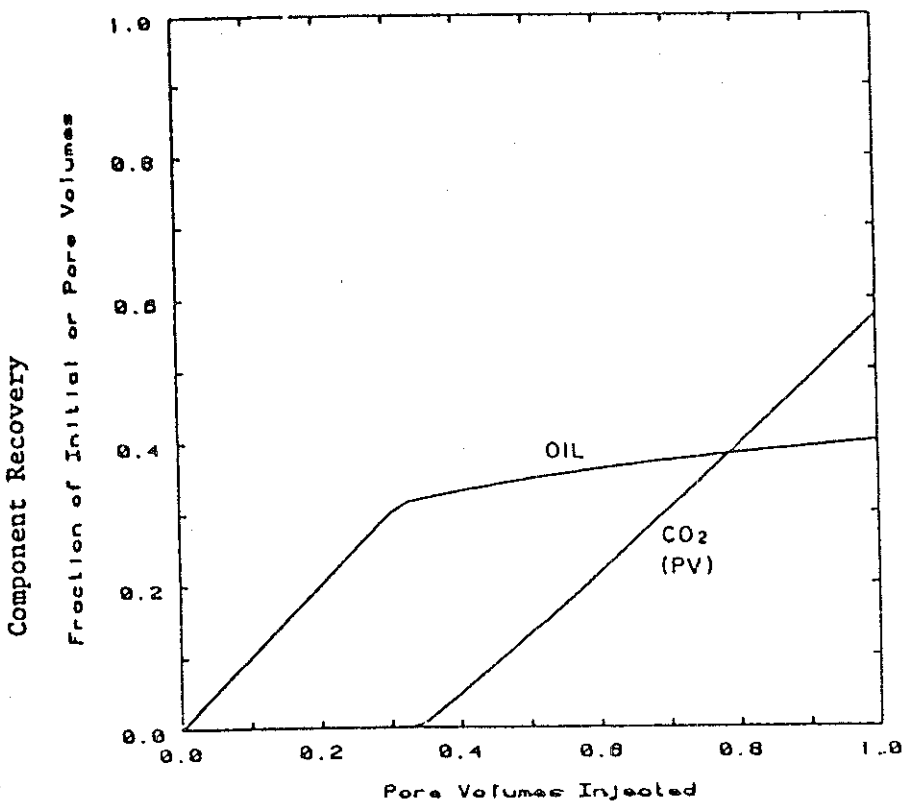

a. 1000 PSI

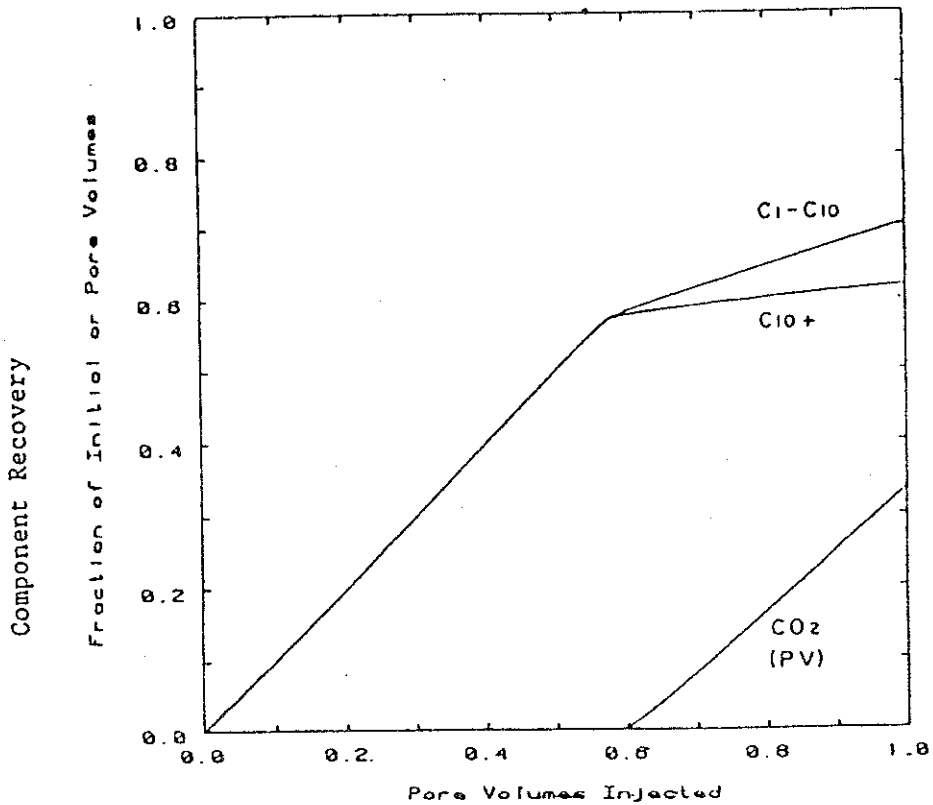

b. 1200 PSI

Figure 33 Calculated recovery of light hydrocarbons (C_1-C_{10}) and heavy hydrocarbons (C_{10+}) for phase diagrams shown in Figure 30.

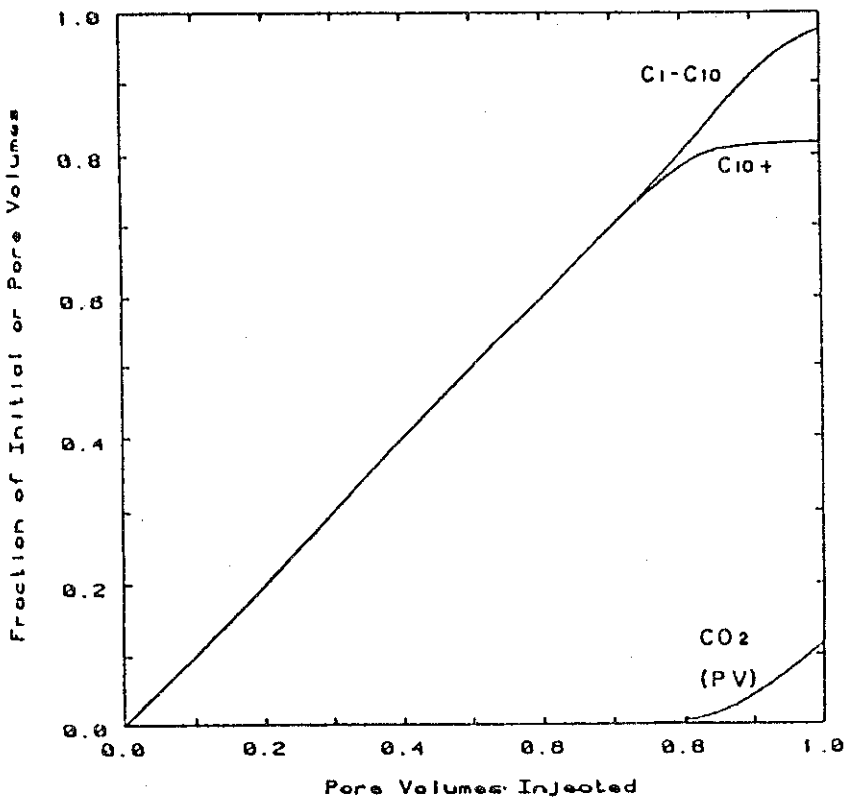

c. 1300 PSI

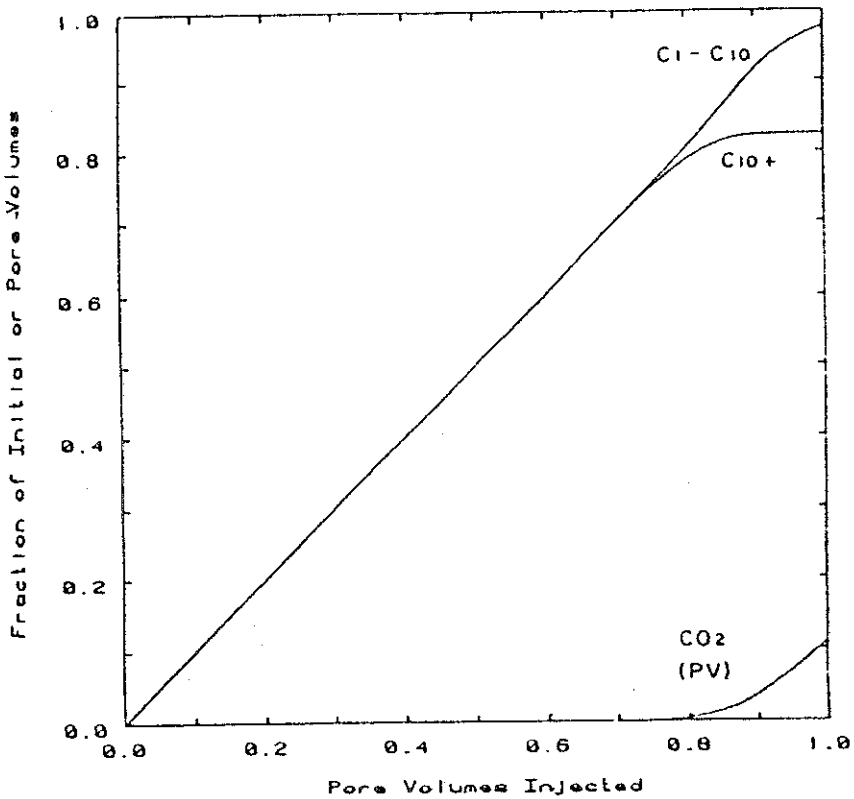

d. 1400 PSI

Figure 33 (continued)

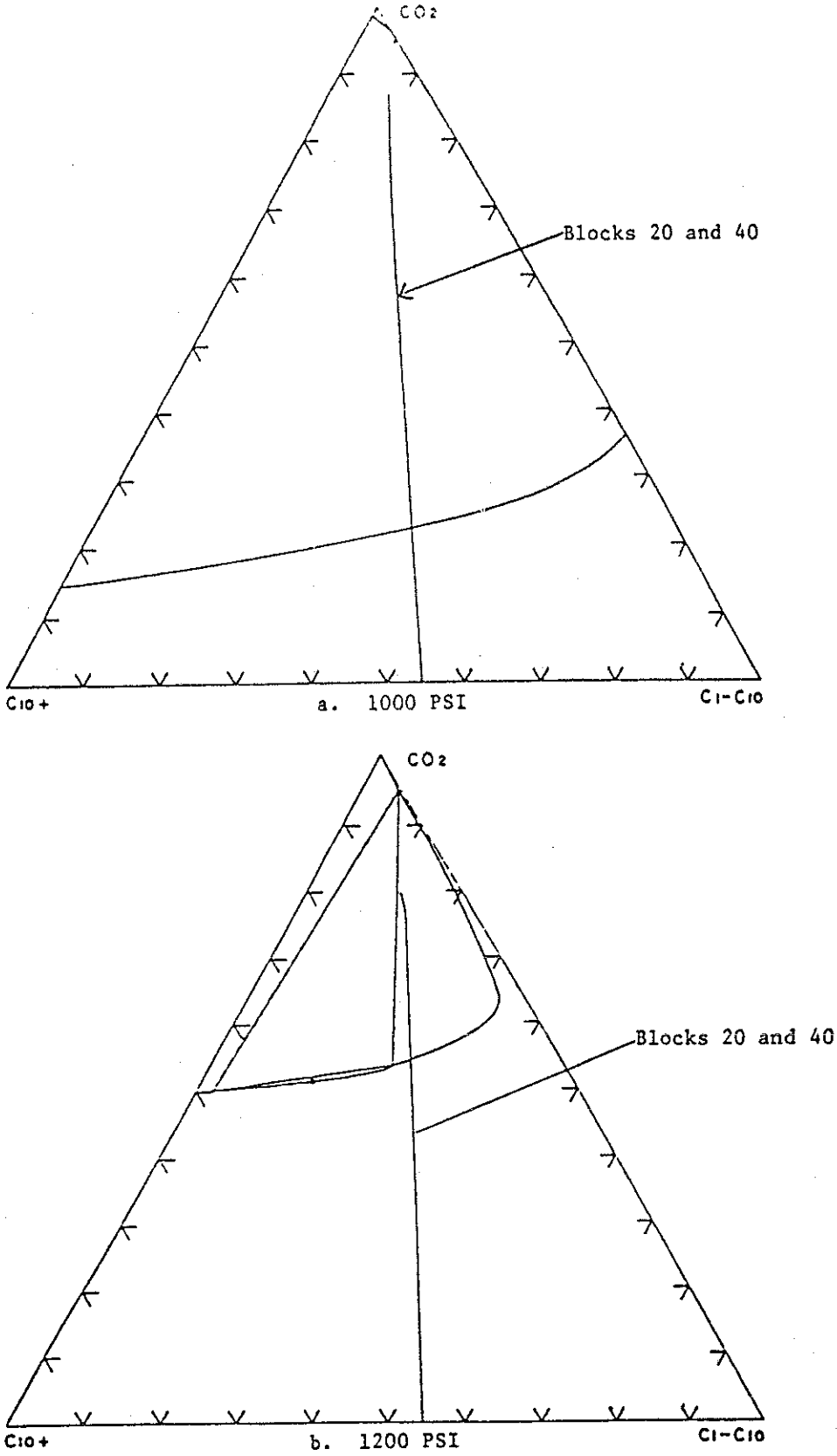

Figure 34 Overall composition paths for middle (block 20) and outlet (block 40) grid blocks. Grid block compositions show substantial enrichment in C_1-C_{10} at 1300 and 1400 psi.

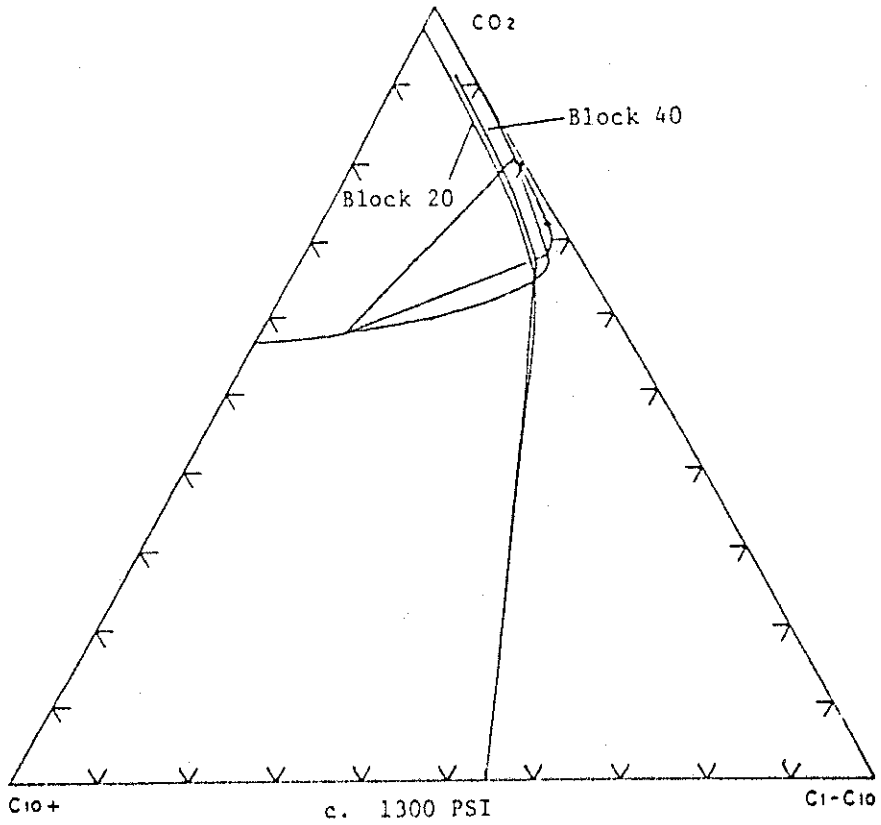

c. 1300 PSI

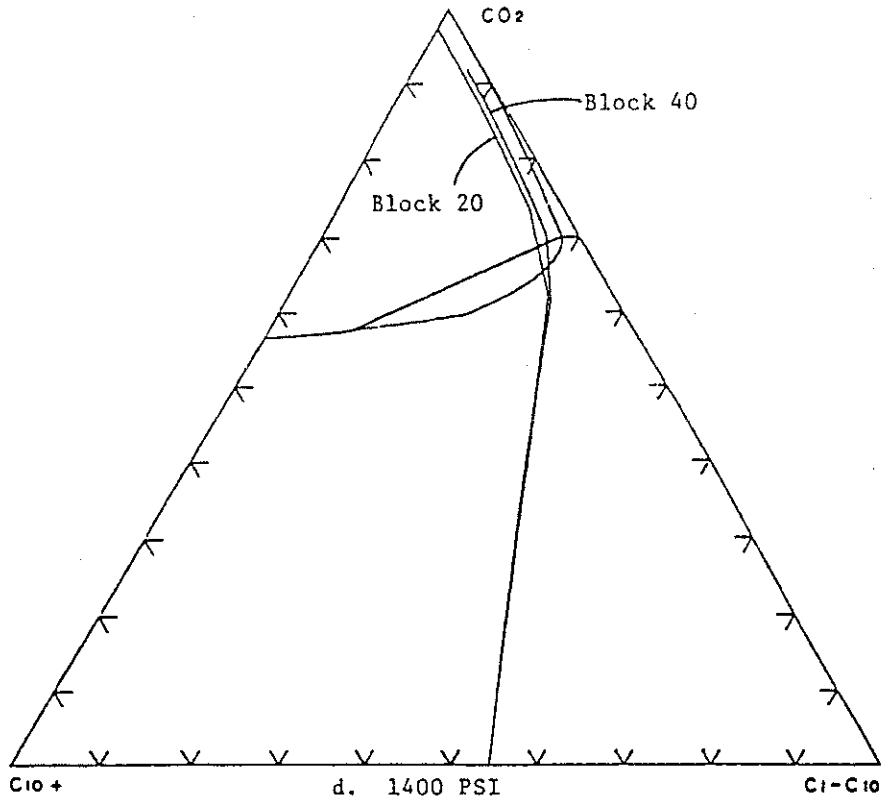

d. 1400 PSI

Figure 34 continued

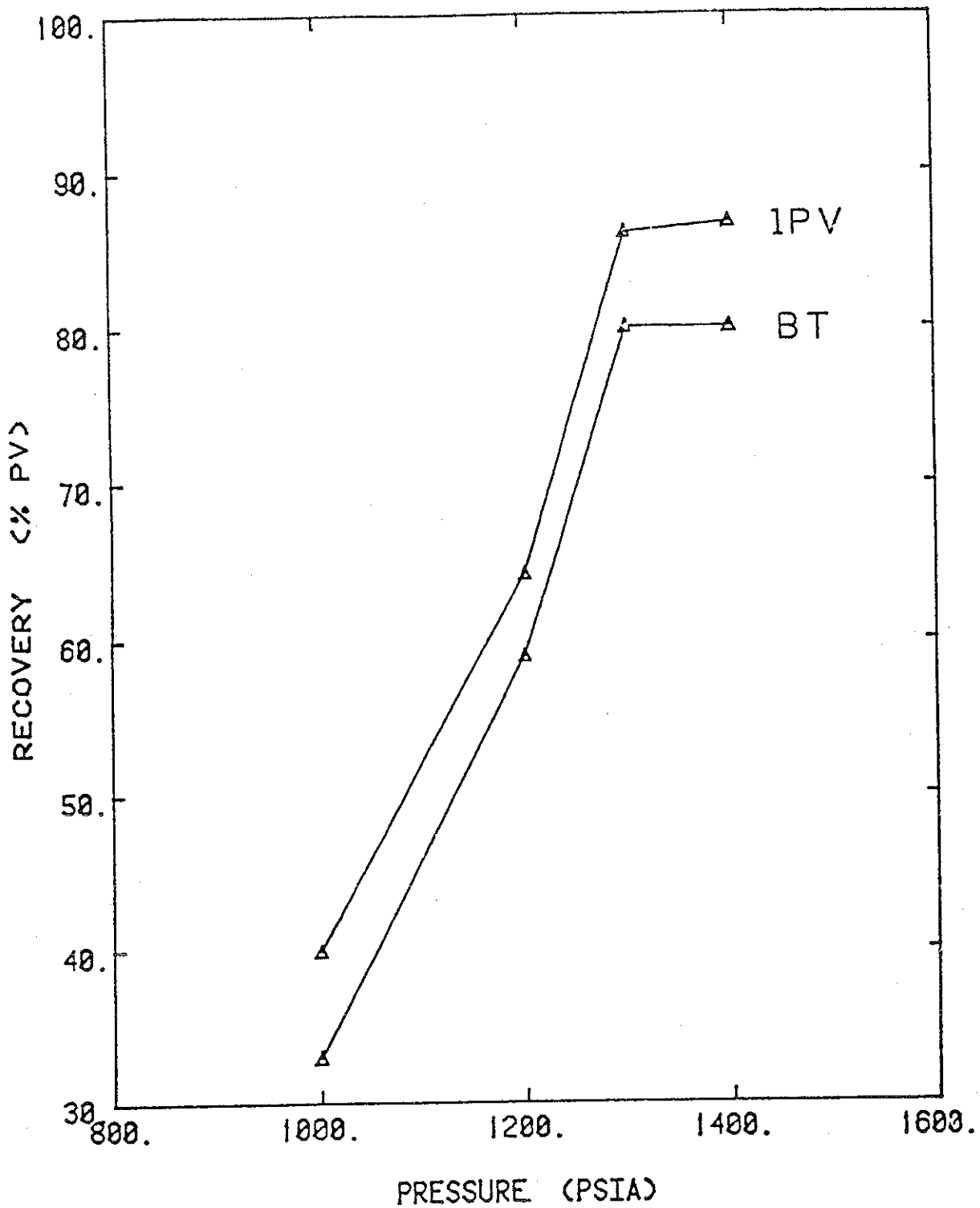

Figure 35 Recovery efficiency at breakthrough (BT) and at one pore volume injected (1PV) for phase diagrams shown in Figure 30.

generation of an efficient displacement has occurred in the inlet region and is developing only slightly in the downstream region. The displacement at 1400 psi shows little change from that 1300 psi because the tie line slopes have changed little, even though the three phase region has disappeared.

Effect of Dispersion

The displacements at 1300 and 1400 psi developed miscibility by a vaporization or extraction mechanism, enrichment of the CO_2 rich phase with C_1-C_{10}. The fact that overall compositions pass through the two and three phase regions is a consequence of dispersion as indicated by the work of Helfferich[34] and Hirasaki.[35] The runs discussed above were made with an inverse Peclet number of 10^{-2} estimated from equation (7). If the inverse Peclet number is reduced to 2×10^{-3}, the 1400 psi displacement produces results shown in Figure 36. Breakthrough is delayed from 0.8 PV to 0.9 PV, and the recovery at 1 PV injected is 93.5% vs. 86.7% previously. Thus, recovery efficiency depends on coupled effects of phase behavior and dispersion. Because field inverse Peclet numbers are often near 10^{-2}, it is reasonable to conclude that some residual to CO_2 will be observed, even when phase behavior is very favorable. Furthermore, because it alters composition paths, dispersion whether physical in a displacement experiment, or numerical in simulations, can obscure conclusions about phase behavior if the effects of dispersion are not accounted for. Thus, considerable caution must be used in concluding whether a flood developed miscibility solely on the basis of recovery efficiency.

Conclusions

While work continues to generate phase diagrams which are completely consistent with experimental observations and to provide additional experimental verification of the phase behavior of CO_2-crude oil mixtures, the following conclusions can be drawn from research to date:

(1) Liquid-liquid and liquid-liquid-vapor separations observed for CO_2-crude oil mixtures are consistent with the phase behavior of CO_2 and normal alkanes.

(2) Liquid-liquid-vapor separations in crude oil-CO_2 systems occur when liquid-vapor separations for CO_2 and light components occur at pressures near those at which liquid-liquid separations occur for CO_2 and the heavy components.

(3) Because CO_2 exhibits liquid-liquid separations with hydrocarbons heavier than C_{13}, essentially all crude oils can be expected to show liquid-liquid and liquid-liquid-vapor behavior for temperatures somewhat above the critical temperature of CO_2.

(4) Extraction of hydrocarbon components by liquid CO_2 rich phases can generate miscibility in the same way that a vaporizing gas drive does.

(5) Some residual oil saturation can be expected in any CO_2 flood even when phase behavior is very favorable because dispersion is always present in field displacements.

(6) High levels of physical or numerical dispersion can obscure the effect

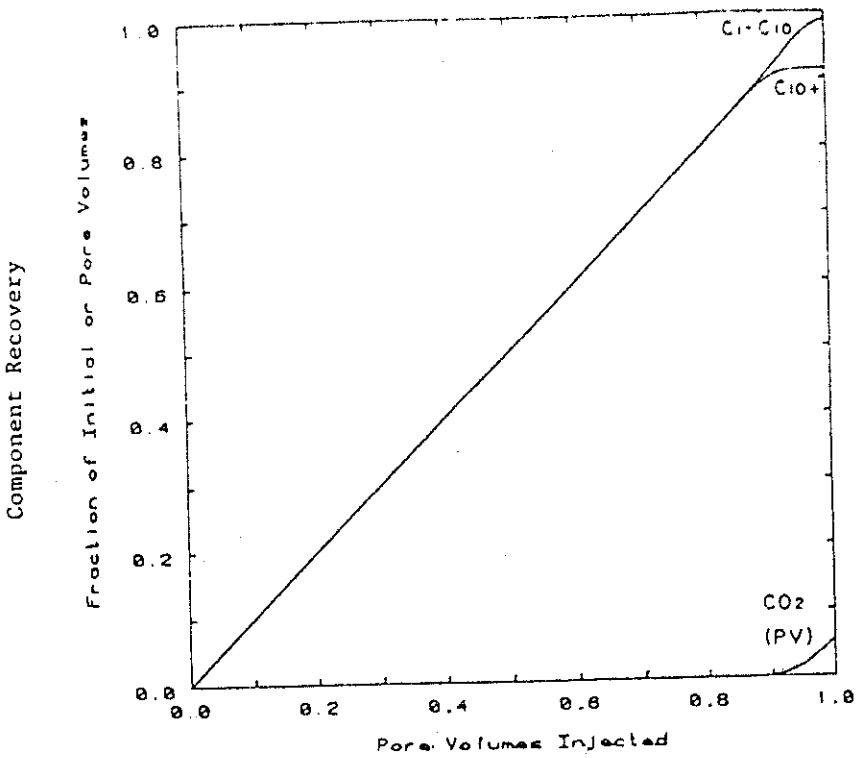

a. Component recovery with low dispersion.

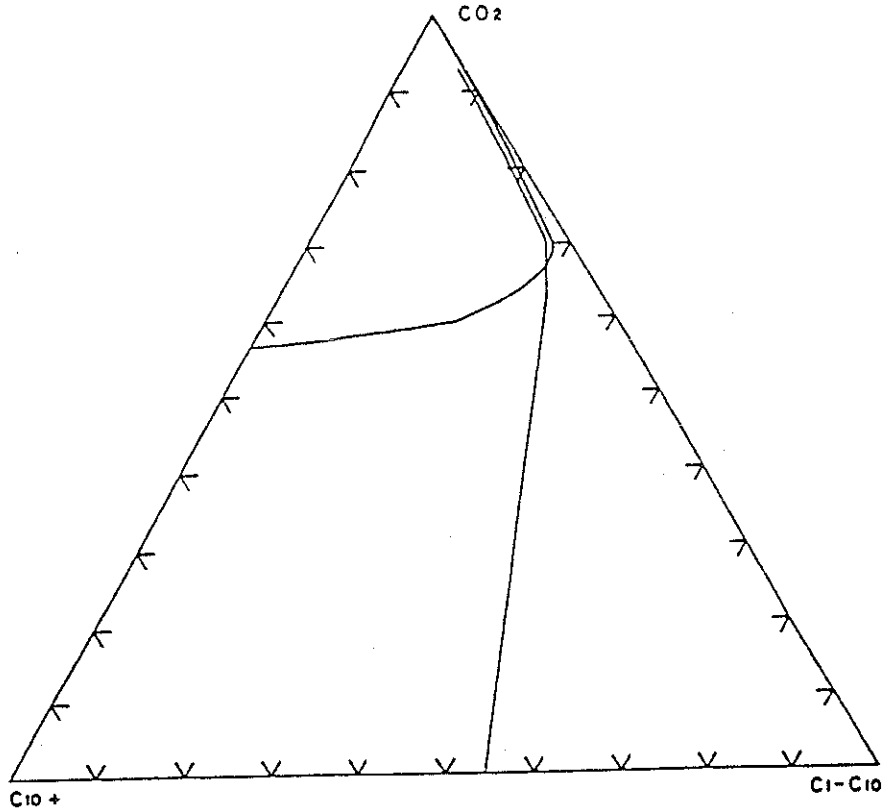

b. Overall composition path for block 40 with low dispersion.

Figure 36. Effect of a five fold reduction in dispersion on component recovery and composition path in the outlet grid block (block 40).

of phase behavior on displacement efficiency. Recovery efficiency alone is a poor measure of the effects of phase behavior unless the effect of dispersion is accounted for.

References

1. Gardner, J.W., Orr, F.M. and Patel, P.D., "The Effect of Phase Behavior on CO_2 Flood Displacement Efficiency," SPE 8367, presented at 54th Fall Technical Conference of SPE of AIME, Las Vegas, Sept. 23-26, 1979.

2. Metcalfe, R.S. and Yarborough, L., "The Effect of Phase Equilibria on the CO_2 Displacement Mechanism, Soc. Pet. Eng. J. 19, 242-252, 1979.

3. Kamath, K.I., Comberiati, J.R. and Zamerilli, A.M., "The Role of Reservoir Temperature in CO_2 Flooding," presented at the Fifth Annual DOE Symposium, Enhanced Oil & Gas Recovery & Improved Drilling Technology, Tulsa, Aug. 22-24, 1979.

4. Holm, L.W. and Josendal, V.A., "Mechanisms of Oil Displacement by Carbon Dioxide," J. Pet. Tech. 16, 1427-1438, 1974.

5. Rathmell, J.J., Stalkup, F.I. and Hassinger, R.C., "A Laboratory Investigation of Miscible Displacement by Carbon Dioxide, Water and Methane," SPE 3483,presented at the 40th Fall Meeting of SPE of AIME, New Orleans, October 3-6, 1971.

6. Simon, R., Rosman, A. and Zana, E., "Phase Behavior Properties of CO_2-Reservoir Oil Systems," SPE 6387, presented at the 52nd Fall Technical Conference of SPE of AIME, Denver, Oct. 9-12, 1977.

7. Huang,E.T.S. and Tracht, J.H., "The Displacement of Residual Oil by Carbon Dioxide," SPE 4735, presented at the SPE-AIME Third Symposium on Improved Oil Recovery, Tulsa, April, 1974.

8. Simon, R. and Graue, D.J., "Generalized Correlations for Predicting Solubility, Swelling and Viscosity Behavior of CO_2-Crude Oil Systems," J. Pet. Tech. 7, 102-106, 1965.

9. Watkins, R.W., "A Technique for the Laboratory Measurement of Carbon Dioxide Unit Displacement Efficiency in Reservoir Rock," SPE 7474, presented at the 53rd Annual Fall Technical Conference of SPE of AIME, Oct. 1-3,1978.

10. Shelton, J.L. and Yarborough, L., "Multiple Phase Behavior In Porous Media During CO_2 or Rich-Gas Flooding," J. Pet. Tech. 19, 1171-1178, 1977.

11. Fussel, L.T., "A Technique for Calculating Phase Equilibria of Three Coexisting Hydrocarbon Phases." SPE 6722, presented at the 52nd Annual Fall Technical Conference of SPE of AIME, Denver, Oct. 9-12, 1977.

12. Boiling Range Distribution of Petroleum Fractions by Gas Chromatography, ASTM Standards, Part 24, 789-797, 1976.

13. Peng, D.Y. and Robinson, D.B., "A New Two-Constant Equation of State," I & EC Fund. 15, 59-64, 1976.

14. Todd, M.R., "Modeling Requirements for Numerical Simulation of CO_2 Recovery Processes," SPE 7998, presented at the 5th SPE Symposium on Reservoir Simulation, Denver, Jan. 31-Feb.2, 1979.

15. Coats, K.H., "An Equation of State Compositional Model," SPE 8284, presented at the 54th Fall Technical Conference of SPE of AIME, Las Vegas, Sept. 23-26, 1979.

16. Fussell, L.T. and Fussell, D.D., "An Iterative Sequence for Phase Equilibria Calculations Incorporating the Redlich-Kwong Equation of State," Soc. Pet. Eng. J., 18, 173-182, 1978.

17. Leach, M.P. and Yellig, W.F., Compositional Model Studies: CO_2-Oil Displacement Mechanisms, SPE 8368, presented at the 54th Fall Technical Conference of SPE of AIME, Las Vegas, Sept. 23-26, 1979.

18. Pope, G.A. and Nelson, R.C., "A Chemical Flooding Compositional Simulator," Soc. Pet. Eng. J. 18, 339-354, Oct., 1978.

19. Nelson, R.C. and Pope, G.A., "Phase Relationships in Chemical Flooding," Soc. Pet. Eng. J. 18, 325-338, Oct. 1978.

20. Nelson, R.C., "Further Studies on Phase Relationships in Chemical Flooding," presented at the 3rd International Conference of Surface and Colloid Science, Stockholm, Sweden, Aug.20-25, 1979.

21. Dietrich, J.K. and Bondor, P.L., "Three-Phase Oil Relative Permeability Models," SPE 6044, presented at the 51st Annual Fall Conference of SPE of AIME, New Orleans, Oct. 3-6, 1976.

22. Stone, H.L., "Estimation of a Three-Phase Relative Permeability and Residual Oil Data," J. Can. Pet. Tech., 12, No. 4, 1973.

23. Todd, M.R. and Longstaff, W.J., "Application of a Numerical Simulator for Predicting Miscible Flood Performance," J. Pet. Tech., 874, July 1972.

24. Lantz, R.B., "Quatitative Evaluation of Numerical Diffusion (Truncation Error)," Soc. Pet. Eng. J., p. 315, Sept. 1971.

25. Firoozabadi, A. and Katz, D.L., "Predicting Phase Behavior of Condensate/Crude Oil Systems Using Methane Interaction Coefficients," J. Pet. Tech., 30, 1649-1655, 1978.

26. Graue, D.J. and Zana, E., "Study of a Possible CO_2 Flood in the Rangely Field, Colorado," SPE 7060, presented at the 5th Symposium on Improved Oil Recovery of SPE-AIME, Tulsa, April 16-18, 1978.

27. Perry, G.E., Guillory, A.J., Baron, J.D., Johnston, J.R. and Moranville, M.B., "Weeks Island 'S' Sand Reservoir B Gravity Stable Miscible CO_2 Displacement," Iberia Parish, Louisiana, presented at the 4th Annual DOE Symposium on Enhanced Oil and Gas Recovery, August 29-31, 1978.

28. Stalkup, F.I., "Carbon Dioxide Miscible Flooding: Past, Present and Outlook for the Future," J. Pet. Tech., 30, 1102-1112, 1978.

29. Schneider, G., "Phase Equilibria in Binary Fluid Systems of Hydrocarbons with Carbon Dioxide, Water and Methane," Chemical Engineering Progress Symposium Series, No. 88, 64, 9-15, 1968.

30. Stewart, W. and Neilson, F.T., "Phase Equilibria for Mixtures of Carbon Dioxide and Several Normal Saturated Hydrocarbons," Prod. Monthly, 27-32, Jan. 1954.

31. Liphard, K.G. and Schneider, G.M., "Phase Equilibria and Critical Phenomena in Fluid Mixtures of Carbon Dioxide + 2, 6, 10, 15, 19, 23-hexamethyltetracosane up to 423°K and 100 MPA," J. Chem. Thermodynamics, 7, 805-814, 1975.

32. Meldrum, A.H. and Nielson, R.F., "A Study of Three-Phase Equilibria for Carbon Dioxide-Hydrocarbon Mixtures," Prod. Monthly, 22-35, Aug. 1955.

33. Elgin, J.C. and Weinstock, J.J., "Phase Equilibria at Elevated Pressures in Ternary Systems of Ethylene and Water with Organic Liquids, Salting Out with a Supercritical Gas," J. Chem. Eng. Data, 4, 3-12, 1959.

34. Helfferich, F.G., "General Theory of Multicomponent, Multiphase Displacement in Porous Media," SPE 8372, presented at the 54th Annual Fall Technical Conference of SPE of AIME, Las Vegas, Sept. 23-26, 1979.

35. Hirasaki, G.J., "Application of the Theory of Multicomponent, Multiphase Displacement to Three Component, Two Phase Surfactant Flooding," SPE 8373, presented at the 54th Annual Fall Technical Conference of SPE of AIME, Las Vegas, Sept. 23-26, 1979.

36. Naar, J., Wygal, R.J. and Henderson, J.H., "Imbibition Relative Permeability in Unconsolidated Porous Media," Soc. Pet. Eng. J., 2, 13-17, 1962.

37. Blackwell, R.J., "Laboratory Studies of Microscopic Dispersion Phenomena," Soc. Pet. Eng. J., 2, 1-8, 1962.

Research Participants

Name	Title	Training	Research Activities
F.M. Orr	Principal Investigator	Ph.D., Chemical Engineering	Project Management, Interaction of phase behavior with flow in porous media.
J.J. Taber	Principal Investigator	Ph.D., Chemistry	Senior Advisor on all aspects of project.
A.D. Yu	Research Engineer	Ph.D., Chemical Engineer	High pressure phase behavior and fluid property measurements. Prediction of phase behavior with equation of state.
C.L. Lien	Research Chemist	Ph.D., Chemistry	Chromatography for crude oil systems. Displacement experiments. Mobility control for CO_2 displacement.
A. Firoozabadi	Visiting Scholar	Ph.D., Gas Engineering	Pseudo-component representation of CO_2 crude oil systems. Equation of state calculations of phase behavior. Simulation of flow with phase behavior. Displacements in fractured reservoirs
H.K.Wainwright	Instrumentation Specialist	B.S., Geology	High pressure equipment design, construction and testing. Instrumentation. Electronics.
M.K. Silva	Laboratory Technician	B.S., Basic Science	Equipment Assembly. High pressure displacement experiments.
R.K. Spaulding	Laboratory Technician	M.S., Chemistry	High pressure phase behavior and fluid property measurements.
S. Pongpitak	Graduate Student	M.S. Candidate, Pet. Eng.	Analogue fluid displacements.
K.D. Rowlison	Undergraduate Research Assistant	Senior, Petroleum Eng.	Core holder design and construction, core displacements.
M.T. Pelletier	Undergraduate Research Assistant	Senior, Metallurgy	High pressure equipment construction, sampling systems, materials compatability.
R.B. May	Undergraduate Research Assistant	Sophomore, Computer Science	Data acquisition and processing for gas chromatography. Digitizer, plotter software.
H.A. Rowlison	Undergraduate Research Assistant	Freshman, Petroleum Eng.	Equipment construction, distillations, low pressure fluid property measurements.

☆ U. S. GOVERNMENT PRINTING OFFICE: 1980—671-115/71

END

DATE FILMED

04/22/80